

## Hydrogenic Stark effect: Properties of the wave functions

David A. Harmin

Department of Physics, University of Chicago, Chicago, Illinois 60637

(Received 2 March 1981)

A modified WKB treatment of a hydrogenic atom in a static electric field  $F$  is found accurate over *all* energies  $\epsilon$  to within 1% for  $F \leq 5000$  kV/cm. This semianalytical technique describes the two properties of the wave function most relevant to photoionization and scattering: (1) the *ratio of amplitudes* at large and small distances  $A_{n,m}(\epsilon, F)$ , and (2) the *asymptotic phase shift*  $\delta_{n,m}(\epsilon, F)$ . The photoionization cross section from the ground state, given as a semianalytical function of  $\epsilon$  and of the quantum numbers  $m$  and  $n$ , describes the polarization-dependent shape resonances observed *above* the zero-field ionization threshold ( $\epsilon = 0$ ) and agrees with the exact calculations of Luc-Koenig and Bachelier. Complex-contour integration of WKB phase integrals reveals an *equipartition of phase* between the two sides of the potential barrier formed by the Coulomb and Stark fields. The total phase shift increases by  $2\pi$  (not  $\pi$ ) between successive quasistationary levels of constant  $n, m, F$ . The WKB method originally applied to the Stark effect by Lanczos and generalized by Miller and Good is reviewed in an appendix.

### I. INTRODUCTION

Recent experiments on the Stark effect of atomic spectra have demonstrated regular modulations in the photoionization cross section near and *above* the zero-field ionization threshold ( $\epsilon = 0$ ) of Rydberg atoms.<sup>1</sup> These results have stimulated research on the Stark effect in a variety of contexts with different theoretical techniques.<sup>2-11</sup> The present study reports several novel features that have emerged for the case of hydrogen itself. We shall focus on the two quantities that are most relevant to the calculation of the absorption spectrum and of scattering: (1) the *ratio of amplitudes* of the wave function in the limits of large and small distances  $A_{n,m}$ , and (2) its conjugate quantity, the *asymptotic phase shift*  $\delta_{n,m}$ . Possibly more important and timely is the opportunity to assemble in a unified treatment the earlier and newer developments on hydrogenic Stark effect wave functions, as a preliminary step towards a full treatment of nonhydrogenic systems by quantum-defect procedures.<sup>12</sup>

The dc Stark effect of Rydberg levels involves an electron in the presence of a static electric field  $F$  and of a Coulomb potential. This situation prevails *outside* the core of a singly excited atom or ion in an external electric field; in this region the potential due to the core electrons departs negligibly from a Coulomb law. The properties of the electron's wave function  $\psi$  in this combined hydrogenic plus Stark potential differ markedly from the purely Coulombic case. Because the Stark potential eventually dominates at large distances from the core,  $\psi$  has a continuum character at any energy  $\epsilon$ : the hydrogenic bound states are shifted in energy and acquire a finite lifetime, or are ionized altogether. Furthermore,  $\psi$  behaves asymptotically like an Airy function, whose phase

and amplitude are modified from a pure-Stark Airy function by the core's Coulomb attraction.

The quantum-defect theory (QDT) approach<sup>13</sup> exploits the simple nature of the potential outside a multielectron core. Its aim is to compactly describe the core's effect on the bound or continuum states of an excited electron in terms of a small set of parameters. These parameters are of three distinct types: (a) those due to an asymptotic potential  $v_p(\vec{r})$ , which has a simple structure and leads to known analytical solutions; (b) those due to the core's medium-range "optical" potential  $v(\vec{r})$  which deviates from  $v_p(\vec{r})$ , but only at shorter ranges; (c) those due exclusively to the short-range effects of the core (including interchannel couplings), which may be expressed as a reaction matrix defined at the core boundary  $\Sigma$ . The effects of the optical potential can be represented by shifts of the phase and amplitude of the asymptotic solution. The core effects are represented instead by boundary conditions at the interface  $\Sigma$  imposed on the external wave function. In Ref. 13 (referred to as GFS) Greene, Fano, and Strinati have outlined a general form of the QDT for any optical potential. They explicitly work out the cases where the optical potential reduces to  $v_p(\vec{r}) \propto -1/r^p$  ( $p=0, 1, 2$ ). In the context of QDT, our Coulomb plus Stark potential is asymptotically purely Stark, while the Coulomb potential  $v_c(\vec{r})$ , together with the centrifugal effects, now plays the role of the optical-potential modification

$$v(\vec{r}) = v_c(\vec{r}) + Fz \xrightarrow{r \rightarrow \infty} v_s(\vec{r}) = Fz.$$

In this paper, we shall not consider the short-range core parameters but rather focus our attention on the asymptotic amplitude and phase of the wave function for the optical potential  $v_c(\vec{r}) + Fz$ .

We shall examine these asymptotic properties in the WKB approximation. In 1930, Lanczos first used WKB phase integrals to study the Stark-shifted discrete spectrum of hydrogen.<sup>14</sup> These integrals all reduce to complete elliptic integrals, which are easy to calculate and whose analytic properties are well known. Moreover, the WKB approximation turns out to depart but little from numerical solutions (Sec. IV D), not just for small fields which perturb the discrete spectrum weakly, but for *arbitrary F over practically the entire energy domain*. This fact will allow us to obtain the asymptotic wave function in terms of elliptic integrals with suitable corrections. The reliability of the method will be investigated particularly where the WKB approximation is expected to break down, namely, when two classical turning points draw close together (near potential extrema).

In contrast to perturbative treatments of the hydrogen spectrum in an electric field,<sup>6,7,9</sup> the method to be used here involves *no* expansions in powers of  $F$  and covers all energies in a uniform way. We will *not* focus attention on a very precise numerical calculation of the energy levels and lifetimes of the lower-lying quasibound states of hydrogen (briefly discussed in Sec. IV E), since this particular problem has been adequately treated by Damburg and Kolosov<sup>7</sup> using a numerical approach. Rice and Good<sup>8</sup> and Bailey *et al.*<sup>9</sup> have applied a modified WKB treatment to find the positions and half-widths of the upper-lying nearly ionized levels of hydrogen; many elements of these works will be borrowed here. Blosssey<sup>4</sup> numerically calculated the Stark effect on photoabsorption by Wannier excitons; Ref. 4 serves as a basis for many of the results contained in Ref. 11 and in this work. More recently, Luc-Koenig and Bachelier<sup>11</sup> have calculated the Stark effect in hydrogen near and above the ionization limit in greater detail by numerical methods. The present work should serve to illustrate their results semi-analytically and adapt them for QDT application, particularly the photoionization cross section (Sec. IB). Some well-known material has been included to make this paper more nearly self-contained.

#### A. Analytical framework

The three-dimensional Schrödinger equation for our problem

$$\left(-\frac{1}{2}\nabla^2 - Z/r + Fz\right)\psi(\vec{r}) = \epsilon\psi(\vec{r}), \quad (1)$$

is separable in parabolic coordinates ( $\xi = r + z$ ,  $\eta = r - z$ ) with the ansatz

$$\psi(\xi, \eta, \phi) = (\xi\eta)^{-1/2}\chi_1(\xi)\chi_2(\eta)e^{im\phi}(2\pi)^{-1/2} \quad (m = 0, \pm 1, \pm 2, \dots). \quad (2)$$

(Atomic units are used here and throughout; we assume  $m \geq 0$ .) In Eq. (1),  $Z$  is the net charge of the core,  $\epsilon$  is the electron energy with respect to the ionization threshold when  $F = 0$ , and the field  $F$  is directed along the  $+z$  axis. The resulting one-dimensional equations for  $\xi$  and  $\eta$  are<sup>15</sup>

$$\frac{d^2\chi_1(\xi)}{d\xi^2} + \left[\frac{1}{2}\epsilon - 2\left(\frac{m^2 - 1}{8\xi^2} - \frac{\beta_1}{2\xi} + \frac{F}{8}\xi\right)\right]\chi_1(\xi) = 0, \quad (3a)$$

$$\frac{d^2\chi_2(\eta)}{d\eta^2} + \left[\frac{1}{2}\epsilon - 2\left(\frac{m^2 - 1}{8\eta^2} - \frac{\beta_2}{2\eta} - \frac{F}{8}\eta\right)\right]\chi_2(\eta) = 0, \quad (3b)$$

with the "effective charges"  $\beta_i$  constrained by

$$\beta_1 + \beta_2 = Z. \quad (4)$$

The boundary condition at  $\xi = 0$  is  $\chi_1 = 0$  and similarly for  $\eta$ . For  $\xi \sim 0$  and  $\eta \sim 0$ , regular solutions of Eqs. (3) are

$$\chi_1(\xi \sim 0) = \xi^{1/2+m/2}[1 + O(\xi)], \quad (5a)$$

$$\chi_2(\eta \sim 0) = \eta^{1/2+m/2}[1 + O(\eta)], \quad (5b)$$

with *energy-independent* normalization.

The potentials in Eqs. (3a) and (3b) (see Fig. 1) differ in the sign of the Stark potential,  $+\frac{1}{4}F\xi$  and  $-\frac{1}{4}F\eta$  (dashed lines in Fig. 1) and this determines the qualitative difference of the separate factors  $\chi_1(\xi)$  and  $\chi_2(\eta)$ . For any  $\epsilon$  the  $\xi$  mode has a classically inaccessible region as  $\xi \rightarrow \infty$ , so  $\chi_1(\xi)$  must damp exponentially. On the other hand, there is a potential barrier in  $\eta$ , peaked at the critical energy  $\epsilon = \epsilon_c < 0$ , with a classically "open" region as  $\eta \rightarrow \infty$  (for negative or very small  $\beta_2$  the potential hump disappears entirely). For given  $F$  and  $\beta_2 > 0$  the energy  $\epsilon_c \approx -2(\beta_2 F)^{1/2} < 0$  is known as the

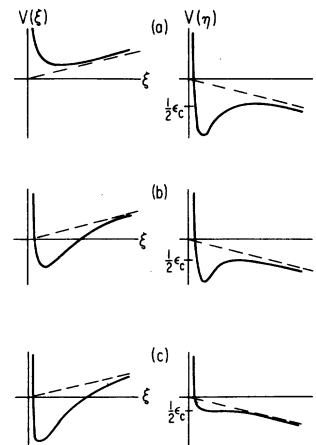


FIG. 1. Qualitative plots of the potentials  $V(\xi)$  and  $V(\eta)$  in Eqs. (3a) and (3b) for  $m > 1$ ,  $F \geq 0$ , and sample values of  $\beta_1 = 1 - \beta_2$ : (a)  $\beta_1 \approx -0.1$ , (b)  $\beta_1 \approx +0.4$ , and (c)  $\beta_1 \approx 0.9$ . --- pure-Stark potentials  $+\frac{1}{4}F\xi$  and  $-\frac{1}{4}F\eta$ . The top of the potential hump in  $\eta$ ,  $\frac{1}{2}\epsilon_c$ , and the potential well coalesce in (c), where  $\beta_2 \approx \beta_{\text{crit}} \sim 0.1$ .

classical ionization limit and marks the barrier peak. Thus, all continuum behavior of the total wave function  $\psi$  must reside in  $\chi_2(\eta)$ , which is to say that ionization of the electron always occurs towards the deepening Stark potential  $z \rightarrow -\infty$ . The problem as defined by Eqs. (3) and the boundary conditions (5) now divides into two problems linked by the constraint (4) as follows: (a) quantization of the bound  $\chi_1(\xi)$  at fixed  $\epsilon$ , i.e., determination of its eigenvalues  $\beta_1$ , and (b) characterization of the asymptotic form of  $\chi_2(\eta)$ , all as a function of the energy  $\epsilon$  and of the field  $F$ . Although Eq. (1) is separable, Eqs. (3a) and (3b) cannot be solved exactly in terms of elementary functions.

Problem (a) is addressed in Sec. II. From the QDT point of view, a bound state in the  $\xi$  mode must have precisely an integral number  $n_1 + 1$  of half-wavelengths between  $\xi = 0$  and  $\xi = \infty$ , separated by  $n_1$  nodes ( $n_1 = 0, 1, 2, \dots$ ). In hydrogen  $n_1$  remains a good quantum number, but in other atoms different  $n_1$  channels are mixed by short-range interactions in the core.<sup>12</sup> We proceed, then, by explicitly considering only single-electron atoms with nuclear charge  $Z = 1$ , where the Coulomb plus Stark potential pertains to *all* space. The results will be incorporated in a subsequent application to nonhydrogenic atoms.

In a WKB approximation the total phase of  $\chi_1(\xi)$  is accumulated between classical turning points  $\xi_1$  and  $\xi_2$ , with an additional contribution of  $\frac{1}{4}\pi$  from each of the two classically inaccessible regions  $\xi \sim 0$  and  $\xi \sim \infty$ . (The case where no such region occurs near  $\xi \sim 0$  will be discussed in the context of the Langer correction in Sec. II.) For fixed  $F$  the quantization of  $\beta_1(\epsilon, F; n_1, m)$  is then determined implicitly by

$$\pi^{-1} \int_{\xi_1}^{\xi_2} k(\xi') d\xi' = n_1 + \frac{1}{2}. \quad (6)$$

The eigenvalues  $\beta_1(\epsilon, F; n_1, m)$  will be accurate insofar as the WKB approximation for the wave number  $k(\xi)$  [see Eq. (23)] is accurate between  $\xi_1$  and  $\xi_2$ , which will be so to  $O(10^{-3})$ .

The asymptotic WKB solutions of Eq. (3b) are derived in Sec. III. Once the  $\beta_1(\epsilon, F; n_1, m)$  are found via Eq. (6), the  $\beta_2(\epsilon, F; n_1, m)$  are given in turn by Eq. (4) and serve as the input to problem (b). Asymptotically,  $\chi_2(\eta)$  must be proportional to a linear combination of the base set of independent Airy functions  $\text{Ai}(w(\eta))$  and  $\text{Bi}(w(\eta))$ ,<sup>16</sup> which are appropriate to the pure-Stark potential dominating at very large  $\eta$ . The Airy functions are solutions of the equation [cf. Eq. (3b)]

$$\frac{d^2 \text{Ai}(w)}{dw^2} + w \text{Ai}(w) = 0, \quad (7)$$

$$w(\eta) = (\frac{1}{4}F)^{1/3}(\eta + 2\epsilon/F);$$

the Airy origin  $w = 0$  lies at  $\eta_A = -2\epsilon/F$  (dashed lines in Fig. 1). We define the energy-normalized<sup>17</sup> combination of this set which vanishes at  $\eta = 0$ :

$$\text{Ci}(\eta) = 2^{1/2}(\frac{1}{4}F)^{-1/6} [\cos \delta_A \text{Ai}(w(\eta)) + \sin \delta_A \text{Bi}(w(\eta))] \\ \rightarrow \left( \frac{2}{\pi k_A(\eta)} \right)^{1/2} \sin[\zeta(\eta) + \frac{1}{4}\pi + \delta_A], \quad (8a)$$

where

$$\zeta(\eta) = \frac{2}{3} |w|^{3/2} = \frac{1}{3} F^{1/2} |\eta + 2\epsilon/F|^{3/2}, \quad (8b)$$

and

$$k_A(\eta) = \frac{d\zeta(\eta)}{d\eta} = (\frac{1}{4}F)^{1/3} w^{1/2} = (\frac{1}{4}F\eta + \frac{1}{2}\epsilon)^{1/2} \quad (8c)$$

is the Airy wave number. The phase shift  $\delta_A$ , required to ensure regularity and positive slope at  $\eta = 0$  consistent with Eq. (5b), must be a smooth function of  $\epsilon$  and  $F$ . It is given in Eq. (8) by

$$\delta_A(\epsilon, F) = -\tan^{-1} \left( \frac{\text{Ai}(w(\eta))}{\text{Bi}(w(\eta))} \right)_{\eta=0}; \quad (9)$$

the branch of the tangent is specified in Appendix B. [One may view  $\delta_A$  as shifting a "zero" of  $\text{Ai}(w(\eta))$  from  $w(\eta = -\infty)$  to  $w(\eta = 0)$ .] It will be convenient later, for the purpose of comparing the asymptotic phase of  $\chi_2(\eta)$  with that of  $\text{Ci}(\eta)$ , to recast the expression (8b) of  $\zeta(\eta)$  as a WKB phase integral

$$\zeta(\eta) = \int_0^{w(\eta)} w'^{1/2} dw' = \int_{\eta_A}^{\eta} (\frac{1}{4}F\eta' + \frac{1}{2}\epsilon)^{1/2} d\eta'. \quad (10)$$

The regular Airy function  $\text{Ci}(\eta)$  serves as the general reference function  $f$  of GFS, which has the asymptotic, energy-normalized form of Eq. (8). As a second independent solution  $g$  with the same normalization, we choose the Airy function that lags  $\text{Ci}(\eta)$  by  $90^\circ$  at large  $\eta$  by setting  $\delta_A \rightarrow \delta_A - \frac{1}{2}\pi$  in Eq. (8).

For future reference we may also define a function in the  $\xi$  mode, analogous to  $\text{Ci}(w(\eta))$  in (8) for the  $\eta$  mode

$$\text{Di}(w(-\xi)) = 2^{1/2}(\frac{1}{4}F)^{-1/6} \text{Ai}(w(-\xi)) \\ \rightarrow \left( \frac{2}{\pi k_A(-\xi)} \right)^{1/2} \frac{1}{2} \epsilon^{-\tau(-\xi)}. \quad (11)$$

$\text{Di}(w)$  satisfies Eq. (7) with  $\eta \rightarrow -\xi$  and vanishes at  $\xi \rightarrow \infty$ .

The wave function  $\chi_2(\eta)$ , distinguished by its energy-independent normalization near  $\eta = 0$  as indicated in Eq. (5b), is a solution of Eq. (3b) for the entire optical potential; hence  $\chi_2(\eta)$  plays the role of  $f^{\text{opt}}$  in Sec. II E of GFS. With this normalization,  $\chi_2(\eta)$  can be represented at any  $\eta$  as a

superposition of the base pair of solutions  $\{f, g\}$  with  $\eta$ -dependent coefficients. In the limit  $\eta \rightarrow \infty$  this superposition takes the same form as the expression (8a) of the wave function  $\text{Ci}(\eta)$  but with different phase and amplitude:

$$\chi_2(\eta) = A_{n_1, m}(\epsilon, F) \left( \frac{2}{\pi k(\eta)} \right)^{1/2} \times \sin \left[ \left[ \xi(\eta) + \frac{1}{4} \pi + \delta_A \right] + \delta_{n_1, m}(\epsilon, F) \right]. \quad (12)$$

Thus, the net effect of the Coulomb well  $-\beta_2/\eta$  plus the centrifugal potential  $\frac{1}{4}(m^2 - 1)/\eta^2$  on  $\text{Ci}(\eta)$  is twofold.

(a) The total phase accumulated by  $\text{Ci}(\eta)$  over the entire interval from  $\eta = 0$  to  $\eta = \infty$  is increased by a finite amount  $\delta_{n_1, m}(\epsilon, F)$ . Although both  $\chi_2(\eta)$  and  $\text{Ci}(\eta)$  have an asymptotically divergent wave number  $k(\eta)$  (which reflects the electron's acceleration in the Stark field), the total phase shift  $\delta_{n_1, m}$  is still well defined as a finite increase of phase expressed as  $\pi$  times the number of additional nodes or half-wavelengths.

(b)  $\chi_2(\eta)$  acquires an energy- and field-dependent amplitude  $A_{n_1, m}(\epsilon, F)$ , in addition to the factor in Eq. (8),  $[2/\pi k_A(\eta)]^{1/2}$ , which is characteristic of WKB solutions.<sup>17</sup> Note that in the limit  $\eta \rightarrow \infty$  the WKB wave number  $k(\eta) = (\frac{1}{4}F\eta + \frac{1}{2}\epsilon)^{1/2}$  is equal to  $k_A(\eta)$  in Eqs. (8c) and (10). The phase and amplitude  $\delta_{n_1, m}$  and  $A_{n_1, m}$  here take the place of the GFS parameters  $\delta_{\epsilon_i}$  and  $\gamma_{\epsilon_i}$  that characterize the asymptotic form of the solution  $f^{\text{opt}}$ .

The phase and amplitude of  $\chi_2(\eta)$  as  $\eta \rightarrow \infty$  also contain the optical effects due to the potential barrier: a partial reflection of  $\chi_2$  above the barrier when  $\epsilon > \epsilon_c$  and a tunneling through the barrier when  $\epsilon < \epsilon_c$ .<sup>5</sup> [We note here that the potential extremum  $\epsilon_c$  depends on  $F, m$ , and  $\beta_2(\epsilon, F; n_1, m)$  and is therefore an implicit function not only of  $n_1$  but also of  $\epsilon$ .] The WKB approximation will require special scrutiny at intermediate energies near the potential lip  $\epsilon \approx \epsilon_c$ . For  $\epsilon < \epsilon_c$ , the total phase shift  $\delta_{n_1, m}$  includes separate contributions from the phase  $\delta_{\text{out}}$  accumulated outside the barrier and the phase  $\delta_{\text{in}}$  accumulated in the inner-well region. Two remarkable features of the WKB phase integrals  $\delta_{\text{out}}$  and  $\delta_{\text{in}}$  and the tunneling integral  $\tau$  will emerge in Sec. III from the analytic structure of these integrals in the complex- $\eta$  plane: (1)  $\tau$  may be expressed in two distinct but equivalent ways as the imaginary part of a complex integral between turning points; (2) for fixed  $m, \beta_2, \epsilon$ , and  $F$ ,  $\delta_{\text{out}}$  exceeds  $\delta_{\text{in}}$  by exactly  $\frac{1}{2}m\pi$ . Therefore, for a given  $n_1$ , the phases  $\delta_{\text{out}}$  and  $\delta_{\text{in}}$  accumulate at an equal rate as  $\epsilon$  increases. The asymptotic phase shift  $\delta_{n_1, m}(\epsilon, F)$  will thus increase by  $2\pi$  between successive quasistationary states

of the inner well, not just by  $\pi$  as one might have expected. It will also be seen that the well and barrier become relatively shallow and localized in energy near  $\epsilon_c$  when the effective charge  $\beta_2$  is very weak compared to a given Stark field  $F$ ; under such circumstances numerical integration of Eq. (3b) seems unavoidable.

The scattering of an Airy wave function from a Coulombic core may be described in terms of the complex Jost functions  $J^\pm$ , which are the coefficients of  $[-2\pi k_A(\eta)]^{-1/2} e^{\pm i\pi} \tau(\eta) \tau^* / 4 + \delta_A^2 \text{Di}(w(-\epsilon))$ . The logarithm of  $J^\pm$  has imaginary and real parts equal, respectively, to (1) the total phase shift of  $\chi_2(\eta), \delta_{n_1, m}(\epsilon, F)$  [see Sec. III B], and (2)  $\ln A_{n_1, m}(\epsilon, F)$  plus a corresponding amplitude factor from the  $\xi$  mode. These two quantities are generally related by a Kramers-Kronig-type dispersion relation in the complex- $\epsilon$  plane.<sup>18</sup> An aspect of this relation will become relevant particularly near quasibound levels in  $\eta$  [see Eq. (47) and Sec. IV, Figs. 6 and 7].

#### B. Photoionization cross section

We consider the photoionization of a hydrogen atom ( $Z=1$ ) in a Stark field  $F$  from its ground state  $|0\rangle$  to excited  $n_1$  eigenstates  $|\epsilon, F; n_1, m\rangle$ . The total cross section  $\sigma_F(\epsilon)$  is a simple sum over the partial cross sections for all  $n_1$  channels

$$\sigma_F(\epsilon) = \frac{4\pi^2}{137} \hbar\omega \sum_{n_1=0}^{\infty} |\langle \epsilon, F; n_1, m | \vec{r} | 0 \rangle|^2, \quad (13)$$

where the absorbed photon energy is  $\hbar\omega = \epsilon - \epsilon_{\text{ground}} = \epsilon + \frac{1}{2}$  a.u.; each term in (13) is identical to the partial density of oscillator strengths of Ref. 11, to within a factor of  $6\pi^2/137$ . The calculation of  $\sigma_F(\epsilon)$  is greatly simplified when we observe that  $|0\rangle$  is concentrated near the nucleus, where the Stark potential is negligible. In this region, the energy-normalized solution of Eq. (1),

$$|\epsilon, F; n_1, m\rangle \approx (N_{\epsilon n_1 m}^F)^{1/2} (\xi\eta)^{1/2m} e^{im\phi} (2\pi)^{-1/2}, \quad r \sim 0 \quad (14)$$

has the same functional form as the purely hydrogenic ( $F=0$ ) solution<sup>19</sup>

$$|\epsilon, 0; n_1, m\rangle \approx (N_{\epsilon n_1 m}^0)^{1/2} (\xi\eta)^{1/2m} e^{im\phi} (2\pi)^{-1/2}, \quad r \sim 0 \quad (15)$$

but differs in its normalization factor  $N_{\epsilon n_1 m}^F$ , to be discussed below. Hence, for the purpose of calculating the squared dipole matrix elements in Eq. (13), we may replace  $|\epsilon, F; n_1, m\rangle$  by  $|\epsilon, 0; n_1, m\rangle$ :

$$|\langle \epsilon, F; n_1, m | \vec{r} | 0 \rangle|^2 = \left( \frac{N_{\epsilon n_1 m}^F}{N_{\epsilon n_1 m}^0} \right) |\langle \epsilon, 0; n_1, m | \vec{r} | 0 \rangle|^2. \quad (16)$$

It is important to note that the zero-field solutions nevertheless depend on the field indirectly through

the value of  $\beta_1(\epsilon, F; n_1, m)$  for each  $n_1$ , which differs from  $\beta_1(\epsilon, 0; n_1, m)$  through the effect of  $F$  at large  $\xi$ . The standard energy-normalization factor for  $|\epsilon, 0; n_1, m\rangle$  is<sup>19, 20</sup>

$$N_{\epsilon n_1 m}^0 = \frac{2}{\nu^{2m+1} m!^2} \binom{n_1+m}{m} \binom{\nu-n_1-1}{m} \\ = \frac{2}{\nu} \begin{cases} 1, & m=0 \\ \beta_1 \beta_2, & m=1 \end{cases} \quad (17)$$

where  $\nu = (-2\epsilon)^{-1/2}$ ,  $n_1 = \beta_1 \nu - \frac{1}{2} m - \frac{1}{2}$  (here  $\epsilon$  is arbitrary, so  $\nu$  is pure imaginary for  $\epsilon > 0$  and is generally irrational).

The azimuthal symmetry of  $\langle \epsilon, 0; n_1, m | \vec{r} | 0 \rangle$  imposes on the transition  $|0\rangle \rightarrow |\epsilon\rangle$  the usual selection rules: (1)  $\pi$  polarization,  $\vec{r} = \vec{z}$ ,  $m=0 \rightarrow m=0$ ; (2)  $\sigma$  polarization,  $\vec{r} = \sqrt{\frac{1}{2}}(\vec{x} \pm i\vec{y})$ ,  $m=0 \rightarrow |m|=1$ ; (3)  $m=0 \rightarrow |m| \geq 2$  not allowed. The zero-field matrix elements  $|\langle \epsilon, 0; n_1, m | \vec{r} | 0 \rangle|^2$  can be evaluated analytically, directly in parabolic coordinates.<sup>21</sup> For future applications,<sup>12</sup> however, it will prove more useful to proceed as follows: (1) calculate the radial (and angular) dipole matrix elements in the energy-normalized spherical basis with the selection rule  $\Delta l = \pm 1$ , and (2) transform to the parabolic basis via the transformation matrix<sup>12, 20</sup>

$$|\langle \epsilon, 0; n_1, m | \epsilon, 0; l=1, m \rangle|^2 \\ = \frac{3\nu}{\nu^2 - 1} \begin{cases} (\beta_1 - \beta_2)^2, & m=0 \\ 2\beta_1 \beta_2, & m=1 \end{cases} \quad (18)$$

This is a purely *geometrical* factor, which shows how  $\beta_1 = 1 - \beta_2$  determines the distribution of  $\psi(\xi, \eta, \phi)$  near the nucleus with respect to the  $z=0$  plane. The dependence on  $m$  results in the striking polarization dependence of  $\sigma_F(\epsilon)$  to be discussed below. The radial and angular integrations<sup>21</sup> give

$$|\langle \epsilon, 0; l=1, m | \vec{r} | 0 \rangle|^2 = \frac{256}{3} \left( \frac{\nu^2}{\nu^2 - 1} \right)^5 \left( \frac{\nu - 1}{\nu + 1} \right)^{2\nu} \quad (19)$$

Collecting the above factors of the dipole integration (16), the photoionization cross section (13) becomes

$$\sigma_F(\epsilon) = \left( \frac{4}{137} \pi^2 \hbar \omega \right) f(\epsilon) \\ \times \sum_{n_1=0}^{\infty} N_{\epsilon n_1 m}^F \begin{cases} [1 - 2\beta_1(\epsilon)]^2, & m=0 \text{ } (\pi) \\ 2, & |m|=1 \text{ } (\sigma) \end{cases} \quad (20)$$

The smooth, analytic function

$$f(\epsilon) = 128(1 + 2\epsilon)^{-6} \\ \times \begin{cases} [(\nu - 1)/(\nu + 1)]^{2\nu}, & \epsilon = -\frac{1}{2} \nu^{-2} \leq 0 \\ e^{-(4/\hbar) \tan^{-1} k}, & \epsilon = \frac{1}{2} k^2 \geq 0 \end{cases} \quad (21)$$

contains all the explicitly energy-dependent fac-

tors [in Eqs. (16)–(19)] of the dipole matrix integration. For  $\epsilon \sim 0$ ,  $f(\epsilon)$  represents the envelope of the zero-field hydrogenic spectrum given in Ref. 21.

The factor  $(1 - 2\beta_1)^2 = (\beta_1 - \beta_2)^2$  arises from the distribution near the nucleus of the Stark effect wave functions with respect to the  $xy$  plane. The  $m=0$  dipole operator  $z$  is odd under reflection through this plane for  $m=0$  and  $\beta_1, \beta_2 > 0$ ; hence, the transition to  $m=0$ ,  $\beta_1 = \beta_2 = \frac{1}{2}$  is forbidden. The resulting parabolic modulation of the intensity  $(1 - 2\beta_1)^2$  is a major feature of the absorption of  $\pi$ -polarized light, emphasized in Ref. 11(c) and emerging *analytically* here.

The factoring out of this slowly varying function of the energy—typical of the QDT approach—focuses attention instead on *channel-dependent* quantities as follows.

(1)  $\beta_1(\epsilon, F; n_1, m)$  governs the size of the potential barriers or wells at small  $\xi$  and  $\eta$  in each  $n_1$  channel and hence determines the distribution and size of the wave function near the nucleus; note, however, that  $\beta_1$  itself is determined by an asymptotic boundary condition on  $\chi_1(\xi \rightarrow \infty)$ .

(2)  $N_{\epsilon n_1 m}^F$ , the *density of states near the origin*, embodies the effects of barrier penetration and potential wells in the energy-normalized wave function (14). Furthermore,  $N_{\epsilon n_1 m}^F$  is also determined by an asymptotic boundary condition, namely, unit outgoing flux in  $\eta$  ( $I_{\text{out}} = 1/2\pi$ ), which effects the normalization of the entire wave function (2) per unit energy range.<sup>15</sup> With  $\chi_1(\xi)$  and  $\chi_2(\eta)$  normalized as in (5), a simple calculation of the flux [see, e.g., p. 3982 of Ref. 4, Appendix 2 of Ref. 11(b), or Sec. IID of GFS<sup>13</sup>] yields

$$N_{\epsilon n_1 m}^F = [A_{n_1 m}(\epsilon, F)]^{-2} \left( \int_0^{\infty} d\xi' \frac{[\chi_1(\xi')]^2}{\xi'} \right)^{-1}, \quad (22)$$

where  $A_{n_1 m}$  is the asymptotic amplitude of  $\chi_2(\eta)$  appearing in Eq. (12).

In the absence of a Stark field, the density of states would depend on  $\epsilon$  smoothly, but any appreciable potential barrier in  $\xi$  or  $\eta$  causes either factor of (22) to decrease exponentially (see Sec. IV C). Such barriers also cause the dependence of  $N_{\epsilon n_1 m}^F$  on  $\beta_1$  to *peak* at  $0 < \beta_1 < 1$  and to vanish rapidly when either  $\beta_1$  or  $\beta_2$  becomes negative (as will be seen in Figs. 3 and 7). In fact, since the range  $0 < \beta_1 < 1$  occurs at higher energies for larger  $F$ ,  $N_{\epsilon n_1 m}^F$  will remain qualitatively similar to  $N_{\epsilon n_1 m}^0$  but be shifted to higher energies. A dominant effect on  $N_{\epsilon n_1 m}^F$  arises, of course, from the barrier in  $\eta$  at  $\epsilon < \epsilon_c$  (see Fig. 1):  $\sigma^F(\epsilon)$  will be vanishingly small here except near quasibound levels, where  $A_{n_1 m}$  goes through a sharp minimum (see Secs. III B and IV E).

The total photoionization cross section (20) has

been calculated for  $F = 1.5 \times 10^{-5}$  a.u. (77 kV/cm) in the WKB approximation as discussed in Secs. II and III. The results were compared with an exact (numerical) calculation of the total density of oscillator strengths by Luc-Koenig and Bachelier,<sup>11(c)</sup> and agreed to within the accuracy of their figures for both  $\pi$ - and  $\sigma$ -polarized light.

Extension of this procedure to initial *excited* states of hydrogen will result in (1) different selection rules for  $\Delta m$  and (2) a different form of  $f(\epsilon)$  (from the dipole matrix integration and coordinate transformation). Both  $N_{\epsilon n_1 m}^2$  and  $\beta_1(\epsilon F; n_1, m)$ , which are parameters of the final-state wave function, will remain unchanged, but the bracketed functions of  $\beta_1$  in Eq. (20) will generally depend on  $m$  (and  $l$ ) through the coordinate transformation (18) and zero-field density of states (17). The initial state  $|nlm\rangle$  must still be low enough in energy, however, to remain concentrated sufficiently near the nucleus for the Stark potential to be negligible; i.e., we must have  $\frac{1}{4}Fr \ll Z/r$  for all  $r \geq Z/|\epsilon| = 2m^2/Z$ , or  $n \ll Z^{3/4}F^{-1/4}$ . Under this condition, a zero-field hydrogenic solution remains a good approximation in Eq. (16).

## II. QUANTIZATION OF $\beta_1(\epsilon, F; n_1, m)$

At each energy  $\epsilon$  and for fixed  $m$  and  $F$  we direct our attention to the eigenvalue spectrum of the effective charge  $\beta_1(\epsilon, F; n_1, m)$  appearing in Eq. (3a). This spectrum is determined as an implicit function of  $\epsilon$  and  $n_1$  by the Bohr-Sommerfeld condition (6). In the WKB approximation the wave number of  $\chi_1(\xi)$  to be entered in Eq. (6) is

$$k(\xi) = \left( -\frac{m^2 - 1}{4\xi^2} + \frac{\beta_1}{\xi} + \frac{1}{2}\epsilon - \frac{1}{4}F\xi \right)^{1/2}, \quad (23)$$

whose integrated phase in the classically accessible region should be a half-integral multiple of  $\pi$  for a bound state.

The validity of the WKB approximation needs to be discussed in two specific areas: (a) for the few smallest values of  $n_1$ , numerical tests are required; the results will be reported at the end of this section; (b) in the region  $\xi \sim 0$ , the assumptions of the WKB approximation break down; however, this difficulty can be bypassed through the Langer correction, which we proceed to discuss.

What is pertinent for our purpose is the accumulation of the phase of  $\chi_1(\xi)$  from  $\xi = 0$  to values of  $\xi \gg 1$  yet small enough so that the term  $\frac{1}{4}F\xi$  in Eq. (23) is negligible. The exact phase accumulation in this range can be read off from the known asymptotic expressions for the Coulomb wave functions, to which  $\chi_1(\xi)$  reduces as long as  $F\xi$  is negligible. This phase is represented by

$$\frac{1}{4}\pi + \int_{\xi_1}^{\xi} \left( -\frac{m^2}{4\xi'^2} + \frac{\beta_1}{\xi'} + \frac{1}{2}\epsilon \right)^{1/2} d\xi', \quad (24)$$

where  $\xi_1$  is the smallest nonnegative zero of the integrand and equals zero for the special case of  $m = 0$ . Note that the centrifugal terms in (24) and (23) differ by  $1/4\xi^2$ . This difference, the Langer correction, results from a procedure which avoids the breakdown of the WKB approximation near  $\xi \sim 0$  by a remapping of the variable  $\xi$  onto  $t = \ln \xi$ , whose range extends to  $t = -\infty$ .<sup>22</sup> [This correction is most familiar in polar coordinates, where it becomes  $l(l+1) \rightarrow (l+\frac{1}{2})^2$ .] The term  $\frac{1}{4}\pi$  in (24) is the phase accrued at  $\xi < \xi_1$ . Accordingly, this term  $\frac{1}{4}\pi$ , combined with an identical term from the exponential tail at large  $\xi$ , contributes to the total phase accumulation but should not be included in Eq. (6) separately [their contribution has already been allowed for in Eq. (6) by entering  $n_1 + \frac{1}{2}$  instead of the actual total number of half-wave-lengths  $n_1 + 1$ ].

On this basis, we can proceed to determine  $\beta_1$  from Eq. (6), which now takes the form

$$\pi^{-1} \int_{\xi_1}^{\xi_2} \left( -\frac{m^2}{4\xi'^2} + \frac{\beta_1}{\xi'} + \frac{1}{2}\epsilon - \frac{1}{4}F\xi' \right)^{1/2} d\xi' = n_1 + \frac{1}{2}, \quad (25)$$

where  $\xi_1$  and  $\xi_2$  are the nonnegative roots of the integrand. The integral in Eq. (25) may be reduced to a complete elliptic integral, which expedites the calculation of  $\beta_1(\epsilon, F; n_1, m)$  considerably. This elliptic expression and a computational procedure are discussed in Appendix C. Appendix C also introduces another correction to the WKB phase integral for Coulomb wave functions,  $\Delta\sigma_m$ ; however, this term is small for  $\epsilon > 0$  and vanishes for  $\epsilon < 0$ .

The results of a calculation for  $F = 1.5 \times 10^{-5}$  a.u. (77 kV/cm) and  $m = 0$  are shown in Fig. 2 but will be discussed in Sec. IV A. Comparison with numerical integration shows that  $\beta_1$  obtained by this procedure is in error by no more than 0.004 for  $n_1 = m = 0$  and for all fields less than 0.001 a.u. (5140 kV/cm). For  $n_1 > 0$  or  $m > 0$  the error is smaller still.

Once  $\beta_1(\epsilon, F; n_1, m)$  has been determined, the integral  $N_{\epsilon} \equiv \left\{ \int_0^{\infty} d\xi' [\chi_1(\xi')]^2 / \xi' \right\}^{-1}$  in the density of states (22) may be evaluated by numerical integration of Eq. (3a)<sup>4,11</sup> or by WKB procedures [see, e.g., Sec. III of Ref. 5(a)]. Figure 3 shows  $\sqrt{N_{\epsilon}}$  for  $m = 0$ ,  $n_1 = 0 - 4$ , and the large field  $F = 0.001$  a.u. The dashed curve at  $\epsilon < 0$  in Fig. 3 is a plot of  $|2\epsilon|^{1/4}$ , which is the exact value of  $\sqrt{N_{\epsilon}}$  for  $F = 0$  and  $m = 0$ , independent of  $n_1$ . For  $F \neq 0$ , the potential well in  $\xi$  exists at all  $\epsilon$ , so the curve for each  $n_1$  extends into the  $\epsilon \geq 0$  domain. In the normal range  $\beta_1 > 0$  (above the crosses in Fig. 3),  $N_{\epsilon}$  remains fairly flat for each  $n_1$  (see Sec. IV C). How-

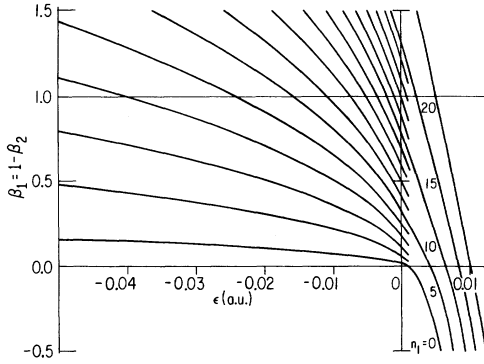


FIG. 2. Eigenvalues  $\beta_1(\epsilon, F; n_1, m) = 1 - \beta_2(\epsilon, F; n_1, m)$  for  $m=0$ ,  $F=1.5 \times 10^{-5}$  a.u. = 77 kV/cm, and  $n_1=0-20$ . Limiting forms are  $\beta_1 \approx (n_1 + \frac{1}{2})(-2\epsilon)^{-1/2}$  for  $\epsilon \ll 0$  and  $\beta_1 \approx -\epsilon^2/4F + (n_1 + \frac{1}{2})\sqrt{\epsilon}$  for  $\epsilon \gg 0$ . Intercepts with  $\beta_2=0$  at  $\epsilon > \sqrt{F}$  and  $\beta_1=0$  at  $\epsilon > 0$  are given in Eqs. (58a) and (58b).

ever, when  $\beta_1$  becomes negative at positive energies (below the crosses),  $N_\xi$  decreases approximately as  $e^{-2\tau}$ , where the tunneling parameter  $\tau \sim \pi |\beta_1| (2\epsilon)^{-1/2}$  measures the effect of the Coulomb barrier in  $\xi$  [cf. Eq. (64c)]. [These features of  $N_\xi$  are complemented by  $A_{n_1 m}^{-2}$  in Eq. (22)—see Fig. 7 in Sec. IV.] For  $m=1$ ,  $N_\xi$  remains similar to the  $m=0$  case but is multiplied by a factor  $|\beta_1|$  for all  $\beta_1 \geq 0$ ; this is discussed in Secs. III B and IV C. A more detailed WKB analysis for  $m=1$  and  $\beta_1 < 0$  actually leads to<sup>23</sup>  $N_\xi \approx e^{-2\tau} \epsilon^{1/2}$ .

### III. ASYMPTOTIC WAVE FUNCTION $\chi_2(\eta)$

The determination of  $\chi_2(\eta \rightarrow \infty)$  in the Coulomb+Stark optical potential of Eq. (3b) rests on the following physical considerations from the introduction.

(a) There is an inner region I where the electric field is negligible and the potential is purely Cou-

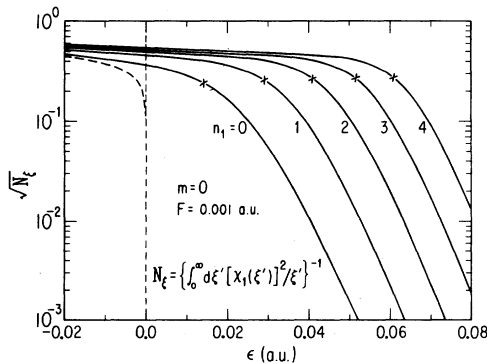


FIG. 3. Factor  $\sqrt{N_\xi}$  in density of states (22), on log scale, vs  $\epsilon$  for  $m=0$ ,  $F=0.001$  a.u. (cf. Fig. 7).  $\times$ :  $\beta_1(\epsilon, F; n_1, 0) = 0$ . ---:  $F=0$ ,  $\sqrt{N_\xi} = |2\epsilon|^{1/4}$ .

lomb plus centrifugal,  $v_1(\eta) = \frac{1}{4} m^2 / \eta^2 - \beta_2 / \eta$ . For moderately large values of  $F$  this region is large enough (e.g., several tens of a.u.) for a WKB-approximated Coulomb wave function to be accurate.

(b) In the asymptotic region (III) the Coulomb field is negligible and the potential reduces to  $v_2(\eta) = -\frac{1}{4} F \eta$ . This consideration motivated the construction in Sec. IA of a regular Airy reference function  $Ci(\eta)$  [Eq. (8a)].

(c) The whole optical potential is relevant in an intermediate zone (region II) that connects the small- and large- $\eta$  regions. This broad region includes the potential barrier and extends in both directions until either the Coulomb or Stark potential sufficiently dominates.

The separation of the entire interval  $0 \leq \eta \leq \infty$  into these three physical regions will facilitate our characterization of the asymptotic phase and amplitude of  $\chi_2(\eta)$  by isolating the influence of distinct physical effects. We will obtain the asymptotic form of  $\chi_2(\eta)$  for fixed  $n_1$ ,  $m$ ,  $\epsilon$ ,  $F$ , and  $\beta_2(\epsilon, F; n_1, m)$  by matching  $\chi_2(\eta)$  from one region to the next, beginning with the wave function specified at  $\eta \sim 0$  in Eq. (5b). For all  $\eta$  except  $\eta \sim 0$ ,  $\chi_2(\eta)$  is to be handled primarily as a WKB solution.

The effects of the potential barrier in region II become negligible at energies far above the barrier peak  $\epsilon \gg \epsilon_c \approx -2\sqrt{\beta_2 F}$  where we may then apply a straightforward WKB solution for the single classically accessible region [see Eq. (48)]. Also, at energies below the bottom of the Coulomb well, the wave function under the barrier is simply a rising exponential, which again matches to a WKB solution in the outer classical region. In these cases, separate treatment of a "region II" is unnecessary. Furthermore, if the separation parameter  $\beta_2 \leq \beta_{\text{crit}} = \frac{3}{4}(m^4 F)^{1/3}$ , there is no potential hump or well at all and a "region II" is again superfluous. However, the WKB method is expected to break down under the joint condition  $\{\beta_2 \approx \beta_{\text{crit}}, \epsilon \approx \epsilon_c\}$ ; in this case the three turning points are not well separated, so the "well" and "barrier" regions themselves are no longer isolated enough to be considered distinct and one must resort to numerical solution of Eq. (3b). The case  $\beta_2 < 0$  will be considered separately at the end of this section.

We discuss some general analytical properties of the WKB phase integrals in the following paragraphs before returning to the region by region matching in Sec. III B.

#### A. Analytical properties of $\int^n k(\eta') d\eta'$

We view here the asymptotic phase shift  $\delta_{n,m}(\epsilon, F)$  as resulting from the development of the WKB phase integral  $\int^n k(\eta') d\eta'$  over the entire domain of  $\eta$  ( $0 \leq \eta \leq \infty$ ). It is therefore important to iso-

late those general properties of  $\delta_{n_1 m}$  which stem from the analytical structure of the WKB phase integrals themselves. An examination of the integral  $\int^\eta k(\eta') d\eta'$  in the complex- $\eta$  plane will be seen to reveal two features that simplify calculations and unify the contributions to  $\delta_{n_1 m}$ .

As discussed in point (a) below Eq. (12),  $\delta_{n_1 m}$  is a phase *shift* which represents the finite difference of the divergent integrals  $\int^\eta k(\eta') d\eta'$  and  $\int^{\eta_A} k_A(\eta') d\eta'$  in the limit  $\eta \rightarrow \infty$  [see Eqs. (10) and (12)]. Hence we wish to consider integrals of the function

$$\delta k(\eta) = k(\eta) - k_A(\eta) \quad (26)$$

over the complex domain of  $\eta$ . The WKB wave number from Eq. (3b), including the Langer correction, is

$$k(\eta) = \left( -\frac{m^2}{4\eta^2} + \frac{\beta_2}{\eta} + \frac{1}{2}\epsilon + \frac{1}{4}F\eta \right)^{1/2} \quad (27)$$

and  $k_A(\eta)$  is given in Eqs. (8c) and (10). We may rewrite Eq. (26) in terms of its four branch points  $a$ ,  $b$ ,  $c$ , and  $\eta_A = -2\epsilon/F = a + b + c$  (see Fig. 4):

$$\delta k(\eta) = \frac{1}{2} \sqrt{F} \left[ [(\eta - a)(\eta - b)(\eta - c)]^{1/2} / \eta - (\eta - \eta_A)^{1/2} \right]. \quad (28)$$

The value of  $\arg[\delta k(\eta)]$  is set to 0 for  $\eta \rightarrow \infty$ . Note that  $\delta k(\eta)$  actually vanishes at  $|\eta| \rightarrow \infty$  as  $|\eta|^{-3/2}$  and has a single simple pole at  $\eta = 0$  with residue  $\frac{1}{2} \sqrt{F} [(-a)(-b)(-c)]^{1/2} = -\frac{1}{2} im$ ; however, the pole turns into a branch point when its residue  $\propto m$  vanishes.

Since  $\delta_{n_1 m}$  will depend on the phase accrued *between* pairs of branch points, we consider for purposes of analysis the integral of  $\delta k(\eta)$  over the entire range from  $\eta = -\infty$  to  $\infty$  broken up into the fol-

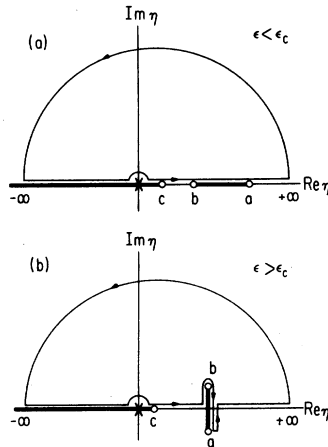


FIG. 4. Contours and branch cuts for loop integrals of  $\delta k(\eta)$ , Eq. (29): (a)  $\epsilon \ll \epsilon_c$ , three real turning points, and (b)  $\epsilon > \epsilon_c$ ,  $b = a^*$ . The pole at  $\eta = 0$  has residue  $-\frac{1}{2} im$ .

lowing pieces:

$$\begin{aligned} \int_{-\infty}^{\infty} \delta k(\eta') d\eta' &= \left( \int_a^{\infty} k(\eta') d\eta' - \int_{\eta_A}^{\infty} k_A(\eta') d\eta' \right) + \int_b^a k(\eta') d\eta' \\ &+ \int_c^b k(\eta') d\eta' \\ &+ \left( \int_{-\infty}^c k(\eta') d\eta' - \int_{-\infty}^{\eta_A} k_A(\eta') d\eta' \right). \quad (29) \end{aligned}$$

Important relationships among these pieces emerge by considering the integral along the *closed* contour shown in Fig. 4(a) for  $\epsilon \ll \epsilon_c$  and in Fig. 4(b) for  $\epsilon > \epsilon_c$ . This contour is closed in the upper half-plane by a semicircle at  $|\eta| = \infty$ , along which the integral *vanishes* as  $|\eta|^{-1/2}$ . An infinitesimal semicircular detour around the pole at  $\eta = 0$  contributes  $-\pi i(-\frac{1}{2} im) = -\frac{1}{2} m\pi$ . The entire loop integral vanishes, as it encloses no singularities.

In Appendix D, Eq. (29) is resolved into its real and imaginary parts for both  $\epsilon < \epsilon_c$  (below the barrier top) and  $\epsilon > \epsilon_c$  (above the barrier). We describe and label the appropriate segments of Eq. (29) as follows: (a) the phase shift *outside* the barrier

$$\delta_{\text{out}} = \text{Re} \int_a^{\infty} k(\eta') d\eta' - \int_{\eta_A}^{\infty} k_A(\eta') d\eta', \quad (30)$$

(b) the tunneling integral

$$\tau \equiv \pi\alpha = \text{Im} \int_b^a k(\eta') d\eta', \quad (31)$$

(c) the phase accumulated in the *inner* well

$$\delta_{\text{in}} = \left| \text{Re} \int_c^b k(\eta') d\eta' \right|, \quad (32)$$

and (d) an alternative tunneling integral

$$\tau' = \text{Im} \left( -\wp \int_{-\infty}^c k(\eta') d\eta' + \int_{-\infty}^{\eta_A} k_A(\eta') d\eta' \right), \quad (31')$$

where  $\wp$  stands for "principal value." In either case  $\epsilon \gtrsim \epsilon_c$ , the vanishing of the entire contour integral gives then

$$\delta_{\text{out}} - \delta_{\text{in}} = \frac{1}{2} m\pi \quad (33)$$

for the real part and

$$\tau = \tau' \quad (34)$$

for the imaginary part.

Equation (33) relates the phases accumulated in the two *separate*, classically accessible physical regions. That  $\delta_{\text{out}}$  and  $\delta_{\text{in}}$  differ by a *constant* independent of both the energy and the field reflects the qualitative, logarithmic nature of the integral over a Coulomb potential<sup>24</sup>; that  $\delta_{\text{out}} - \delta_{\text{in}}$

amounts to *exactly*  $m$  quarter wavelengths is attributable to the centrifugal barrier singularity. This remarkable *equipartition* property of the phases will manifest itself in  $\delta_{n_1 m}(\epsilon, F)$  as an increase of  $2\pi$  between successive quasistationary states; each successive bound state must accumulate not only an extra half-wavelength in the well but an equal amount *outside* the barrier as well.

The initial form (31) of the tunneling integral reduces to an elliptic integral readily only for energies below the barrier top,  $\epsilon < \epsilon_c$ . On the other hand, its form (31'), which results from our analysis, reduces to that form for all  $\epsilon$ . Below the barrier  $\tau$  has its usual interpretation as a tunneling parameter; its extrapolation to the range above the barrier, where it follows an imaginary path and is *negative*, will serve to single out the diffractive effect of the barrier. This extrapolation has been indicated previously,<sup>5, 25</sup> but the interconnection of the parameters by the loop integration of Fig. 4 is new and extends the extrapolation to the case of  $m \neq 0$ .

The forms of the elliptic integral expressions for  $\tau$  and  $\delta_{in} = \delta_{out} - \frac{1}{2} m\pi$  are shown in Table I. They depend on the positions of  $a$ ,  $b$ , and  $c$  in the complex- $\eta$  plane. Below the barrier top ( $\epsilon < \epsilon_c$ ) and above the bottom of the Coulomb well all three roots are real and nonnegative (*case 1*). The phase shift will depend on  $\delta_{in}$  and  $\tau$  alone. Above the barrier ( $\epsilon > \epsilon_c$ ) there is a single classically accessible region with a single nonnegative turning point  $c$ ;  $a$  and  $b$  are either complex conjugate (*case 2*) or both real and negative (*case 3*). The

phase shift for this region is

$$\begin{aligned} \delta_{\text{clas}} &\equiv \int_c^\infty k(\eta') d\eta' - \int_{\eta_A}^\infty k_A(\eta') d\eta' \\ &= \delta_{in} + \delta_{out} \end{aligned} \quad (35)$$

from which we readily obtain  $\delta_{out}$  and  $\delta_{in}$  by Eq. (33).

We list the expressions for  $\tau$  and  $\delta_{in}$  (or  $\delta_{\text{clas}}$ ) in Table I as variants of a single functional form

$$\begin{aligned} \delta \text{ or } \tau &= (F\mathcal{P}_0)^{-1/2} \left\{ \frac{2}{3}(\epsilon\mathcal{P}_1 \pm 4\beta_2)K(k) - \frac{2}{3}(\epsilon\mathcal{P}_2)E(k) - \frac{2}{3}(\epsilon\mathcal{P}_2)E(k) \right. \\ &\quad \left. + m^2[\mathcal{P}_3\Pi(n, k) - \mathcal{P}_4K(k)] \right\}, \end{aligned} \quad (36)$$

where the five constants  $\mathcal{P}_i$  are algebraic combinations of  $a$ ,  $b$ , and  $c$ ;  $K$ ,  $E$ , and  $\Pi$  are the three canonical forms of complete elliptic integrals.<sup>26</sup> For given  $m$ ,  $F$ ,  $\epsilon$ , and  $\beta_2(\epsilon, F; n_1, m)$ , the roots  $a$ ,  $b$ , and  $c$  are determined by the cubic equation (27). When  $m=0$  these expressions simplify considerably [as does Eq. (C3)—see Appendix C].

#### B. Asymptotic phase and amplitude; optical effects

In this section we give a three-step procedure to obtain  $\chi_2(\eta \rightarrow \infty)$  in the form of Eq. (12): (1) in region I, obtain the energy-normalized solution for  $\eta \sim 0$ ; (2) in region II, determine the large- $\eta$  form of this solution via a WKB connection formula across the potential barrier, thereby incorporating into  $\chi_2(\eta)$  the optical effects of the barrier; (3) in region III, compare  $\chi_2(\eta)$  to the Airy reference function  $\text{Ci}(\eta)$  of Eq. (8a) to obtain the asymptotic phase and amplitude.

TABLE I. Elliptic-integral expressions for  $\delta_{in}$  [Eq. (32)],  $\delta_{\text{clas}}$  [Eq. (35)], and  $\tau$  [Eq. (31) or (31')]. General form, Eq. (36):

$$\begin{aligned} \delta &= (F\mathcal{P}_0)^{-1/2} \left\{ \frac{2}{3}(\epsilon\mathcal{P}_1 + 4\beta_2)K(k) - \frac{2}{3}(\epsilon\mathcal{P}_2)E(k) + m^2[\mathcal{P}_3\Pi(n, k) - \mathcal{P}_4K(k)] \right\}, \quad 0 < k^2 < n < 1 \\ \tau &= (F\mathcal{P}_0)^{-1/2} \left\{ \frac{2}{3}(\epsilon\mathcal{P}_1 - 4\beta_2)K(k') - \frac{2}{3}(\epsilon\mathcal{P}_2)E(k') + m^2[\mathcal{P}_3\Pi(n, k') - \mathcal{P}_4K(k')] \right\}, \quad 0 < n < k'^2 = 1 - k^2 < 1 \end{aligned}$$

		$\mathcal{P}_0$	$\mathcal{P}_1$	$\mathcal{P}_2$	$\mathcal{P}_3$	$\mathcal{P}_4$	$k^2$	$n$
Case 1 ( $\epsilon < \epsilon_c$ )	$\delta_{in}$	$a - c$	$a$	$a - c$	$\frac{1}{a} - \frac{1}{b}$	$\frac{1}{a}$		$\frac{a(b-c)}{b(a-c)}$
	$0 \leq c < b < a$	$\tau$	$a - c$	$-c$	$a - c$	$\frac{1}{a}$	$\frac{b-c}{a-c}$	$\frac{a-b}{a}$
Case 2 ( $\epsilon > \epsilon_c$ ) $0 \leq c$	$b = a^* = b_1 + ia_1$	$\delta_{\text{clas}}$	$A$	$A + c$	$2A$	$-\frac{(A+c-b_1)(A-c)}{ a ^2(A+c)}$	$\frac{b_1}{ a ^2}$	$\frac{ a ^2}{(A+c)^2}$
	$ b ^2 =  a ^2 = b_1^2 + a_1^2$ $A \equiv [(b_1 - c)^2 + a_1^2]^{1/2}$	$\tau$	$A$	$A - c$	$2A$	$\frac{A-c}{2c(A+c)}$	$\frac{1}{2c}$	$\frac{A-c+b_1}{2A}$
Case 3 ( $\epsilon > 0$ ) $a < b < 0 \leq c$	$\delta_{\text{clas}}$	$c - a$	$c$	$c - a$	$\frac{1}{c}$	$-\frac{1}{c}$	$\frac{b-a}{c-a}$	$-\frac{a}{c-a}$

(1) *Renormalization of  $\chi_2(\eta \sim 0)$ .* The energy-independent wave function for  $\eta \sim 0$  is given in Eq. (5b); from this solution we wish to obtain the corresponding WKB solution for region I. Ignoring  $F$  in region I for  $\beta_2 > 0$  permits us to connect  $\chi_2(\eta \sim 0)$  with a regular, *energy-normalized*<sup>17</sup> Coulomb wave function  $\chi_2^{\text{in}}(\eta)$  through a *known* co-

efficient:

$$\chi_2(\eta) = [B_{n_1 m}(\epsilon)]^{-1/2} \chi_2^{\text{in}}(\eta). \quad (37)$$

With the appropriate substitutions,<sup>27</sup>  $B_{n_1 m}$  is given in Table I of GFS<sup>13</sup> (where it is called  $B$  for  $\epsilon > 0$  and  $A$  for  $\epsilon < 0$ ):

$$B_{n_1 m}(\epsilon) = \begin{cases} \pi^{-1} k^m m!^{-2} e^{\pi\beta_2/k} |\Gamma(\frac{1}{2} + \frac{1}{2}m - i\beta_2/k)|^2, & \epsilon = \frac{1}{2}k^2 > 0 \\ \frac{2\nu^{-m}\Gamma(\beta_2\nu + \frac{1}{2} + \frac{1}{2}m)}{m!^2\Gamma(\beta_2\nu + \frac{1}{2} - \frac{1}{2}m)} = 2\beta_2^m m!^{-2} \prod_{j=0,1/2}^{(m-1)/2} (1 - j^2/\beta_2^2\nu^2), & \epsilon = -\frac{1}{2}\nu^{-2} < 0 \end{cases} \quad (38)$$

the index  $j$  is integral (half-integral) for  $m$  odd (even), and  $\Pi_j = 1$  for  $m = 0, 1$ . [Both expressions (38) reduce to  $2\beta_2^m m!^{-2}$  at  $\epsilon = 0$  if  $\beta_2 > 0$ .] The exact energy-normalized wave function  $\chi_2^{\text{in}}(\eta)$  should be well approximated by the WKB solution for the Coulomb potential in the range  $|\epsilon|^{-1/2} \ll \eta \ll 1/F$ . This energy-normalized WKB solution is

$$\chi_2^{\text{in}}(\eta) = \left(\frac{2}{\pi k(\eta)}\right)^{1/2} \sin\left(\int_c^\eta k(\eta') d\eta' + \Delta\sigma_m + \frac{1}{4}\pi\right), \quad (39)$$

where  $k(\eta)$  is given in Eq. (27) and  $c$  is the smallest nonnegative zero of  $k^2(\eta)$ ;  $\Delta\sigma_m$  is the small phase correction given in (C7) for positive-energy WKB solutions (with  $\beta_1 - \beta_2$ ), and will be omitted in subsequent formulas. With Eqs. (37)–(39),  $\chi_2(\eta)$  is expressed in terms of a WKB integral extending to the barrier's (real or complex) turning point  $b$ :

$$\chi_2(\eta) = [B_{n_1 m}(\epsilon)]^{-1/2} \left(\frac{2}{\pi k(\eta)}\right)^{1/2} \times \cos\left[\left(\text{Re} \int_\eta^b k(\eta') d\eta' + \frac{1}{4}\pi\right) - \delta_{1n}\right], \quad \text{region I, } \eta \ll \text{Re}(b). \quad (40)$$

(2) *Connection to  $\chi_2(\eta \gg a)$ .* The WKB wave function (40) is now taken as the starting point on the small- $\eta$  side of the barrier for a solution in region II. The usual WKB procedure for tunneling through the barrier breaks down near its top. A connection procedure, developed by Miller and Good<sup>5(a)</sup> and reviewed in Appendix A, serves to join the WKB wave function (40) to a correspond-

ing wave function  $\chi_2^{\text{out}}(\eta)$  on the large- $\eta$  side. The appropriate connection formula applies *above* as well as below the top of the barrier throughout the range  $\epsilon \sim \epsilon_c$  where the usual WKB method breaks down. It is derived by mapping a potential barrier with a *pair* of turning points onto a *parabolic* barrier  $V(x) = -\frac{1}{4}x^2$  via a transformation of the independent variable  $\eta \rightarrow x = x(\eta)$ . The connection formula thus derived relates to parabolic cylinder functions, as the usual WKB connection formula across a single linear turning point relates to Airy functions. The mapping onto a parabola disregards the presence of the third turning point  $c$ , which is normally  $\ll \text{Re}(b)$ . The procedure will thus fail near the bottom of the well, a range where  $b \approx c$ ; however, the WKB solution is not reliable here and is not of primary interest to us anyway. The procedure will also fail at  $\epsilon \approx 0$ , where  $\text{Re}(b) \approx c$ , but the diffractive effect of the barrier is then negligible (unless  $\beta_2 \approx \beta_{\text{crit}}$ ). Despite these exceptions, the procedure of Appendix A, in fact, deals adequately with the case of three turning points.

The barrier's diffractive effects on  $\chi_2(\eta)$ —of tunneling for  $\epsilon < \epsilon_c$  and of partial reflection for  $\epsilon > \epsilon_c$ —appear in  $\chi_2^{\text{out}}(\eta)$  as a short-range phase shift  $\gamma_{n_1 m}(\epsilon, F)$  and an amplitude-modulating factor  $R_{n_1 m}(\epsilon, F)$ . These quantities depend entirely on *two* parameters, namely, the *accumulated inner phase*  $\delta_{1n}$  and the *tunneling integral*  $\tau$  of Eqs. (30)–(34). Thus, starting from  $\chi_2(\eta \ll \text{Re}(b))$  as given by Eq. (40) and using Eqs. (A12)–(A20), we find

$$\chi_2(\eta) = [B_{n_1 m}(\epsilon)]^{-1/2} \chi_2^{\text{out}}(\eta) = [B_{n_1 m}(\epsilon)]^{-1/2} R_{n_1 m}(\epsilon, F) \left(\frac{2}{\pi k(\eta)}\right)^{1/2} \sin\left[\left(\text{Re} \int_a^\eta k(\eta') d\eta' + \frac{1}{4}\pi\right) + [\gamma_{n_1 m}(\epsilon, F) + \frac{1}{2}\phi(\tau)]\right], \quad \text{region II, } \eta \gg \text{Re}(a) \quad (41)$$

where

$$\phi(\tau) \equiv \arg\Gamma\left(\frac{1}{2} + i\alpha\right) + \alpha(1 - \ln|\alpha|), \quad \alpha = \tau/\pi \quad (42)$$

$$\gamma_{n_1 m}(\epsilon, F) = \tan^{-1}\left[\tan^2\frac{1}{2}\theta \tan\left(\delta_{1n} + \frac{1}{2}\phi\right)\right], \quad (43)$$

$$R_{n_1 m}(\epsilon, F) = \frac{\cos\left(\delta_{1n} + \frac{1}{2}\phi\right)}{\tan\frac{1}{2}\theta \cos\gamma_{n_1 m}}, \quad (44)$$

and

$$\theta \equiv \tan^{-1}(e^{-\tau}). \quad (45)$$

Equation (43) is complemented by requiring  $\gamma_{n_1 m}$  to lie on the same branch of the tangent as  $\delta_{\text{in}} + \frac{1}{2}\phi$ . The elliptic-integral expressions for  $\delta_{\text{in}}(\epsilon, F; n_1, m)$  and  $\tau(\epsilon, F; n_1, m)$  are summarized in Table I.

Under the barrier,  $\tau > 0$  grows rapidly as  $\epsilon$  decreases below  $\epsilon_c$ , so the tunneling parameter  $\frac{1}{2}\theta \approx \frac{1}{2}e^{-\tau}$  is a very small quantity. Thus,  $\gamma_{n_1 m}$  is significantly nonzero only under the resonance condition  $\delta_{\text{in}} + \frac{1}{2}\phi \approx \frac{1}{2}\pi$ . For fixed values of  $n_1$ ,  $m$ , and  $F$ , the energies  $\epsilon_{n_2}(n_1, m, F)$  at which

$$\delta_{\text{in}} + \frac{1}{2}\phi = \pi(n_2 + \frac{1}{2}), \quad n_2 = 0, 1, 2, \dots, \quad (46)$$

i. e., the centers of these resonances, may be identified as the Stark-shifted *quasibound energy levels* of hydrogen.<sup>11(b)</sup> [For  $\tau = O(1)$ , however, see Sec. IV E.] The positions and widths of these levels for  $\epsilon_{n_2} \approx \epsilon_c$  have been studied by Rice and Good<sup>8</sup> and Bailey *et al.*,<sup>9</sup> and by Damburg and Kolosov<sup>7</sup> for  $\epsilon < \epsilon_c$ . The function  $\frac{1}{2}\phi(\tau)$  defined in Eq. (42) [see also Eq. (A13)] stems from contributions to the phase integrals from the classical turning points and from the asymptotic expansions of the parabolic cylinder functions. In the quantization rule (46),  $\frac{1}{2}\phi(\tau)$  represents a correction to the positions of the quasibound levels due to the finite width of the barrier, a correction that vanishes for  $F=0$ . Note that  $\phi(\tau)$  has precisely the same form as the Coulomb phase correction  $\Delta\sigma_m$  [discussed in Appendix C, see Eqs. (C5)–(C7)] with  $m=0$  if we replace the tunneling parameter

$\alpha = \tau/\pi > 0$  by the Coulomb barrier parameter  $\alpha = \beta_2/k < 0$ .

The factor  $1/R_{n_1 m}$ , which gauges the ratio of amplitudes  $\chi_2(\eta \sim 0)/\chi_2(\eta \gg a)$ , depends strongly on barrier effects. Inside the barrier the wave function is a linear combination of increasing and decreasing exponentials; the former usually dominates at  $\eta \approx a$ , so  $R_{n_1 m}^{-1} \approx \tan \frac{1}{2}\theta \approx \frac{1}{2}e^{-\tau} \ll 1$ . In the vicinity of an energy level  $\epsilon_{n_2}(n_1, m, F)$ , however, the coefficient of the increasing exponential vanishes and a node shoots through the barrier into the inner-well region.<sup>28</sup> This change is manifest in the wave function  $\chi_2(\eta \gg a)$  as  $\gamma_{n_1 m}$  rapidly increases by  $\pi$  and  $R_{n_1 m}^{-1}$  goes through a sharp maximum equal to  $\cot \frac{1}{2}\theta \approx 2e^\tau$ . Near  $\epsilon_{n_2}(n_1, m, F)$ , the phase (43) and amplitude (44) are related by the dispersion formula

$$\frac{d\gamma_{n_1 m}(\epsilon, F)}{d\epsilon} = R_{n_1 m}^{-2}(\epsilon, F) \left( \frac{d\delta_{\text{in}}}{d\epsilon} \right)_{\epsilon=\epsilon_{n_2}}; \quad (47)$$

$\gamma_{n_1 m}$  and  $R_{n_1 m}$  are given in Eqs. (63)–(65) in terms of the quasibound level's width  $\Gamma_{n_2}(n_1, m, F)$ .

The phase shift  $\gamma_{n_1 m}$  increases steadily as a function of the energy as one rises in energy through the barrier peak  $\epsilon = \epsilon_c$ . A possible and important exception to this behavior is the occurrence of a shape resonance at (or just above)  $\epsilon = \epsilon_c$  if Eq. (46) is fulfilled near there. Above the barrier  $\tau$  becomes large and negative and we have  $\frac{1}{2}\theta \rightarrow \frac{1}{4}\pi$  and  $\phi(\tau) \rightarrow 0$ , so  $\gamma_{n_1 m} \rightarrow \delta_{\text{in}}$  and  $R_{n_1 m} \rightarrow 1$ . In this limit Eq. (41) takes the form

$$\chi_2(\eta) = [B_{n_1 m}(\epsilon)]^{-1/2} \left( \frac{2}{\pi k(\eta)} \right)^{1/2} \sin \left( \text{Re} \int_a^\eta k(\eta') d\eta' + \left| \text{Re} \int_c^b k(\eta') d\eta' \right| + \frac{1}{4}\pi \right) \propto \sin \left( \int_c^\eta k(\eta') d\eta' + \frac{1}{4}\pi \right), \quad (48)$$

where we have used Eq. (35) with its integral extending only to finite  $\eta$ . Equation (48) has the form of a WKB solution appropriate to the single classical region  $c < \eta < \infty$  when the effect of the barrier becomes negligible.

(3) *Asymptotic form of  $\chi_2(\eta)$ .* In region III, finally, the wave number  $k(\eta)$  of our wave function (41) approaches its Airy function limit  $k_A(\eta)$ . The function (41) itself reduces to its anticipated form (12) whose phase shift can now be specified as

$$\delta_{n_1 m} = \delta_{\text{out}} + \gamma_{n_1 m}(\epsilon, F) + \frac{1}{2}\phi(\tau) - \delta_A(\epsilon, F). \quad (49)$$

Here the contribution  $\delta_{\text{out}}$  is given by Eq. (30) as the limit of the difference between the phase integral in the wave function (41) and that in the Airy

function;  $\gamma_{n_1 m} + \frac{1}{2}\phi$  stems from Eq. (41) itself and  $-\delta_A$  is the adjustment to the Airy phase given in Eq. (9) and Appendix B. The amplitude  $A_{n_1 m}$  of Eq. (12) is obtained by direct comparison with Eq. (41) as

$$A_{n_1 m} = (B_{n_1 m})^{-1/2} R_{n_1 m}. \quad (50)$$

As noted before, the total phase shift  $\delta_{n_1 m}$  rises by  $2\pi$  in each interval between successive quasibound levels  $\epsilon_{n_2}$ . In Eq. (49) one-half of this rise is contributed by  $\gamma_{n_1 m}$  and occurs abruptly at  $\epsilon_{n_2}$  while the rest is contributed by  $\delta_{\text{out}}$  and accumulates smoothly. Far enough above the barrier, e.g., at  $\epsilon \sim 0$ , Eq. (43) shows that  $\gamma_{n_1 m}$  approaches the value  $\delta_{\text{in}}$  given by Eq. (32); the total phase

shift reduces then to

$$\delta_{n_1 m} = \delta_{in} + \delta_{out} - \delta_A = \delta_{class} - \delta_A, \quad (51)$$

as anticipated in Eq. (35). At the same time  $R_{n_1 m}$  approaches unity and  $A_{n_1 m}$  reduces to  $(B_{n_1 m})^{-1/2}$ .

*Amplitude for  $\beta_2 < 0$ .* A negative value of  $\beta_2$  implies an effective Coulomb repulsion throughout the range  $0 < \eta < \infty$  without any potential hump (i.e., with  $R_{n_1 m} = 1$ ). One must then consider the Coulomb factor  $B_{n_1 m}(\epsilon)$ , Eq. (38), more carefully. For  $\epsilon > 0$ ,  $B_{n_1 m}^{-1}(\epsilon)$  measures the squared amplitude of the zero-field Coulomb wave function at large  $\eta$ , in particular,

$$\begin{aligned} A_{n_1 0}^{-2}(\epsilon, 0) &= B_{n_1 0}(\epsilon) \\ &= 2(1 + e^{-2\pi\beta_2/k})^{-1}, \quad m = 0 \end{aligned} \quad (52a)$$

$$\begin{aligned} A_{n_1 1}^{-2}(\epsilon, 0) &= B_{n_1 1}(\epsilon) \\ &= 2\beta_2(1 - e^{-2\pi\beta_2/k})^{-1}, \quad m = 1. \end{aligned} \quad (52b)$$

The quantity  $-\pi\beta_2/k \equiv \tau_0 > 0$  equals the tunneling integral under the repulsive Coulomb barrier in the absence of centrifugal effects. When  $|\beta_2/k|$  is large, we have  $A^{-2} \propto e^{-2\tau_0}$ , as expected for a tunneling process, and  $\tau_0$  diverges as  $\epsilon \rightarrow 0$ . However, the potential barrier  $|\beta_2|/\eta - \frac{1}{4}F\eta$  has a turning point at any energy, unlike the pure Coulomb barrier, so  $\chi_2(\eta)$  will not diverge even at  $\epsilon < 0$  as  $\eta \rightarrow \infty$ . We proceed to show that (1) the factor  $|\beta_2|^m$  in the functional forms (52) and in Eq. (38) results only from the centrifugal repulsion, represented by  $m$ , and that (2) the exponent  $\tau_0$  may be generalized to a tunneling integral  $\tau$ , which depends on the combined Coulomb plus Stark potential but is independent of centrifugal effects.

We seek the large- $\eta$  amplitude  $A_{n_1 m}(\epsilon, F)$  of a WKB expression for  $\chi_2(\eta)$  with the energy-independent normalization (5b). We begin again at small  $\eta$  by neglecting the potential term  $\frac{1}{4}F\eta$ . Langer has shown<sup>29</sup> that the zero-field Coulomb wave function for  $\beta_2 < 0$  at any  $\epsilon$  can be approximated inside the barrier by a modified Bessel function of order  $m$ , whose argument is a WKB tunneling integral:

$$\chi_2(\eta) = A \left( \frac{\int_0^\eta |k_0(\eta')| d\eta'}{k_0(\eta)} \right)^{1/2} I_m \left( \int_0^\eta |k_0(\eta')| d\eta' \right), \quad F = 0. \quad (53)$$

Here  $k_0(\eta) = [\frac{1}{2}\epsilon - |\beta_2|/\eta]^{1/2}$  is the WKB wave number (27) (for  $F = 0$ ) without the centrifugal term  $m^2/4\eta^2$ . Equation (53) is valid over a large range of  $\eta$ , including  $\eta \rightarrow 0$  but not extending through a turning point of  $k_0(\eta)$ . The coefficient  $A$  is determined by the normalization condition (5b) at  $\eta \rightarrow 0$ , where the integral is  $\approx 2(|\beta_2|\eta)^{1/2}$ ; the low- $z$  form of  $I_m(z \sim 0) = (\frac{1}{2}z)^m m!^{-1} [1 + O(z^2)]$  gives then

$$\chi_2(\eta) \approx A(\sqrt{2}|\beta_2|^{m/2}/m!) \eta^{1/2+m/2} [1 + O(\eta)].$$

The normalization condition (5b) sets  $A = |\beta_2|^{-m/2} m!/\sqrt{2}$ .

For large  $\eta$  [such that  $|k_0^2(\eta)| \gg \frac{1}{4}F\eta$ ], substitution of the asymptotic representation of the Bessel function in Eq. (53) gives

$$\chi_2(\eta) = A \left( \frac{2}{\pi k_0(\eta)} \right)^{1/2} \exp \left( \int_0^\eta |k_0(\eta')| d\eta' \right).$$

Since the exponential form of  $\chi_2(\eta)$  now depends only on the WKB tunneling integral  $\int_0^\eta |k_0(\eta')| d\eta'$ , we may restore the negligible term  $\frac{1}{4}F\eta$  to  $k_0^2(\eta)$  and extend the integral to larger  $\eta$ . Finally, the usual WKB connection formula across a single turning point yields Eq. (12) with  $\delta_{n_1 m}$  given by Eq. (51) and

$$\begin{aligned} A_{n_1 m}^{-2}(\epsilon, F) &= A^{-2} = 2|\beta_2|^m m!^{-2} e^{-2\tau} \\ &= \begin{cases} 2e^{-2\tau}, & m = 0, \\ 2|\beta_2| e^{-2\tau}, & m = 1. \end{cases} \end{aligned} \quad (54)$$

This is smaller than the  $\beta_2 > 0$  form of the Coulomb amplitude  $B_{n_1 m}(\epsilon)$  in Eq. (38) by the factor  $e^{-2\tau}$ , as anticipated, and thus accounts for the sharp cut-offs of the partial densities of state in Eq. (22) when  $\beta_1$  or  $\beta_2 < 0$ . The tunneling integral

$$\tau = \int_0^a (|\beta_2|/\eta' - \frac{1}{2}\epsilon - \frac{1}{4}F\eta')^{1/2} d\eta'$$

is identical to the integral on the left of Eq. (C1) with  $m = 0$ ,  $\beta_1 \rightarrow |\beta_2|$ , and  $\epsilon \rightarrow -\epsilon$ . As compared to numerical calculations for  $F = 0.001$  a.u. and  $m = 0 - 1$ , this method gives  $A_{n_1 m}^{-1}$  with an error on the order of 1% or less if  $|\beta_2| > 0.1$ ; when  $\beta_2 \approx \beta_{crit} \sim 0$ , however, the error may be 10–20%.

#### IV. QUANTITATIVE RESULTS AND DISCUSSION

The eigenvalue curves  $\beta_1(\epsilon, F; n_1, m)$  of Sec. II and the phase  $\delta_{n_1 m}(\epsilon, F)$  and amplitude  $A_{n_1 m}(\epsilon, F)$  of Sec. III are discussed here with regard to their: qualitative features in different regions of  $\epsilon$  (Secs. IVA–IVC), accuracy as functions of  $F$  and  $\epsilon$  as compared with results of numerical integration of Eq. (3b) (Sec. IV D), and prediction of energy levels and ionization rates, though little is added here to previous results (Sec. IV E). In most of the examples discussed in this section we have set  $m = 0$  for simplicity, but the calculations and qualitative observations apply to  $m \neq 0$  as well.

##### A. Eigenvalue curves $\beta_1(\epsilon, F; n_1, m)$

For a given Stark field  $F$  and a given  $m$ , the family of eigenvalue curves  $\beta_1(\epsilon, F; n_1, m)$  vs  $\epsilon$  with

different  $n_1$  forms a smooth monotonically decreasing bundle. Figure 2 shows the lowest  $n_1$  curves for  $F = 1.5 \times 10^{-5}$  a.u. (77 kV/cm) and  $m = 0$ . This figure affords a more compact discussion than has been given previously.

In the  $F = 0$  case, all the curves reduce to parabolas

$$\beta_1(\epsilon, 0; n_1, m) = (n_1 + \frac{1}{2} + \frac{1}{2}m)(-2\epsilon)^{1/2}, \quad (55)$$

which condense to the ionization threshold  $\epsilon = 0$  and do not exist for  $\epsilon > 0$ . When  $F \neq 0$ , however, the motion along  $\xi$  is bounded at nonnegative energies as well. The curves  $\beta_1(\epsilon)$  remain then approximately parabolic for  $\epsilon \ll 0$  but depart increasingly from parabolas at  $\epsilon \sim 0$ , extending into the  $\epsilon > 0$  region, where they drop sharply towards  $\beta_1 \ll 0$ . The first-order correction to  $\beta_1(\epsilon)$  for  $\epsilon \ll -[F(n_1 + \frac{1}{2})]^{2/3}$  raises each parabola by the factor  $1 + \frac{3}{2}F(n_1 + \frac{1}{2} + \frac{1}{2}m)|2\epsilon|^{-3/2}$ , as seen from Eq. (25) or first-order perturbation theory. The limiting behavior of  $\beta_1(\epsilon, F; n_1, m)$  for large  $\epsilon$  follows directly from Eq. (25):

$$\beta_1(\epsilon, F; n_1, m) = \frac{-\epsilon^2}{4F} + \epsilon^{1/2}(n_1 + \frac{1}{2})[1 + O(\alpha_1)], \quad (56)$$

where

$$\alpha_1 \equiv F(n_1 + \frac{1}{2})\epsilon^{-3/2} \ll 1.$$

The broad potential well  $U(\xi) \approx -\beta_1/\xi + \frac{1}{4}F\xi$  has a minimum just below  $\epsilon$  at  $\epsilon_{\min} = 2(-\beta_1 F)^{1/2} \approx \epsilon(1 - 2\alpha_1)$ .

The graph of the eigenvalue curves  $\beta_1(\epsilon)$  in Fig. 2 serves as a basis for conveniently representing the quasibound, Stark-shifted levels of a Rydberg atom. When  $F = 0$  and  $\epsilon < 0$ , we can construct not only the family of eigenvalue curves (55) for the  $\xi$  mode but in addition a corresponding family of  $n_2$  curves for the  $\eta$  mode,

$$\beta_2(\epsilon, 0; n_2, m) = 1 - \beta_1 = (n_2 + \frac{1}{2} + \frac{1}{2}m)(-2\epsilon)^{1/2}. \quad (55')$$

The quantization of both  $\chi_1(\xi)$  and  $\chi_2(\eta)$ , therefore, requires the bound levels for a given  $m$  to lie at the intersection points of (55) and (55'), as shown in Fig. 5(a) for  $m = 0$ . At each energy  $\epsilon = -\frac{1}{2}n^{-2}$  there are  $n - m = n_1 + n_2 + 1$  degenerate levels, which lie on the vertical lines converging to  $\epsilon = 0$  in the figure. The presence of a Stark field  $F \neq 0$  warps this picture, as shown in Fig. 5(b) for  $F = 1.5 \times 10^{-5}$  a.u. and  $m = 0$ . Whereas the  $n_1$  curves are "stretched out" towards  $\epsilon > 0$ , as described above, the  $n_2$  curves (dashed lines) no longer reach their zero-field condensation point  $\epsilon = 0$ . The energy levels ( $n_1 n_2 m$ ) now spread out in energy for each  $n$ —linearly for the lower states in accordance

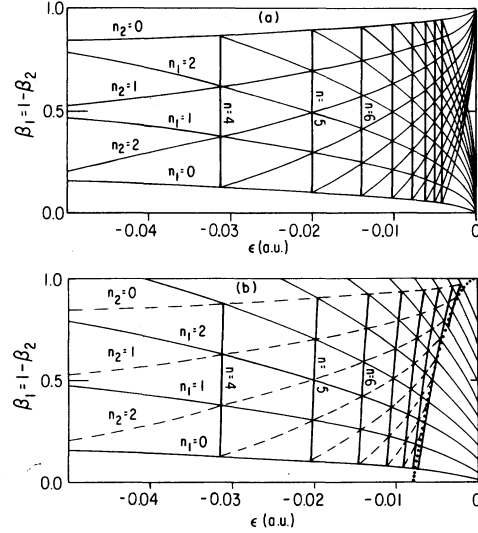


FIG. 5. (a) Eigenvalue curves  $\beta_1(\epsilon)$  and  $\beta_2(\epsilon)$  for  $m = 0$ ,  $F = 0$ , and  $n_1, n_2 = 0-10$ . Vertical lines at  $\epsilon = -\frac{1}{2}n^{-2}$ ,  $n = n_1 + n_2 + 1 = 4-11$ , connect  $n$ -fold degenerate Rydberg levels ( $n n_1 n_2 0$ ), which lie at  $\beta_1 + \beta_2 = 1$  and condense to  $\epsilon = 0$  threshold as  $n \rightarrow \infty$ . (b) Eigenvalue curves  $\beta_1(\epsilon)$  (solid) for  $m = 0$ ,  $F = 1.5 \times 10^{-5}$  a.u. (same as Fig. 2), and  $n_1 = 0-10$ . Dashed curves connect quasibound levels ( $n n_1 n_2 0$ ) of constant  $n_2$ . Stark splitting of  $n = 4-11$  levels is indicated by tilting and bending of vertical lines. Dotted line represents the ionization threshold at the top of the  $\eta$  barrier  $\epsilon_c = -2(\beta_2 F)^{1/2}$ . All states with  $n_1 > 12$  are ionized [Eq. (57)].

with a first-order Stark shift, but nonlinearly for the higher states. The ionization threshold is indicated in Fig. 5(b) by the dotted line which marks the top of the barrier in  $\eta$ , the critical energy  $\epsilon_c$ , where  $\beta_2 = \epsilon_c^2/4F$ . For higher fields the distortion of the eigenvalue curves is magnified, the lines of constant  $n$  become more skewed, and fewer states retain an appreciable lifetime.

The eigenvalue curves in Figs. 2 and 5(b) are also useful in determining which kinds of resonances in the density of states (22) occur in different energy regions. They are as follows.

(a) In the lowest few  $n_1$  curves one finds a range where  $0 < \beta_2 < \epsilon_c^2/4F$ , i.e., where there is an attractive Coulomb potential in  $\eta$  while  $\epsilon$  is still below the barrier top  $\epsilon_c$ . In this region the quasibound states described above give rise to sharp resonances in the density of states. The higher  $n_1$  curves, however, do not attain positive  $\beta_2$  until  $\epsilon > 0$ , which means they cannot yield any quasibound states at all. The lowest value of  $n_1$  for which no such quasibound state occurs follows from Eq. (C3) with  $\beta_1 = 0$ ,  $\epsilon = 0$ ,  $m = 0$ :

$$n_1 + \frac{1}{2} \leq \frac{4K(\sqrt{F})}{3\pi} F^{-1/4} = (0.787)[F(\text{a. u.})]^{-1/4} \\ = (37.5)[F(\text{kV/cm})]^{-1/4}. \quad (57)$$

This form was obtained by Rau<sup>2</sup> with an incorrect additional factor  $\sqrt{\frac{1}{2}}$ .

(b) An additional shape resonance occurs in Eq. (22) above the barrier top for each  $n_1$  in the range  $0 \leq \beta_1 \leq 1$ , but the density of states cuts off exponentially whenever either  $\beta_1$  or  $\beta_2$  become negative, as mentioned in Sec. I B and discussed in Sec.

IV C. The energies at which each  $n_1$  curve intersects these limits in  $\beta_1$  also follow from Eq. (C3). The upper limits—where  $\beta_1 = 0$ —occur at the energy levels of a triangular potential well [dashed line for  $V(\xi)$  in Fig. 1(a)],

$$\beta_1 = 0: n_1 + \frac{1}{2} = \frac{(2\epsilon)^{3/2}}{3\pi F}. \quad (58a)$$

If  $n_1 < 0.8F^{-1/4}$ , the lower limit simply occurs at the barrier top,  $\epsilon_c < 0$ . For larger values of  $n_1$ , however, the lower limit is  $\beta_2 = 0$  at  $\epsilon > 0$ , and one must invert Eq. (C3) with fixed  $n_1$  and  $\beta_1 = 1$  to obtain  $\epsilon$ ; for large  $\epsilon$  this equation becomes

$$\beta_2 = 0: n_1 + \frac{1}{2} = \frac{(2\epsilon)^{3/2}}{3\pi F} \left[ 1 + \frac{3F}{4\epsilon^2} \left( \ln \frac{16\epsilon^2}{F} + 1 \right) - \frac{9F^2}{32\epsilon^4} \left( \ln \frac{16\epsilon^2}{F} - \frac{17}{6} \right) + O\left(\frac{F^3}{\epsilon^6}\right) \right], \quad \epsilon > \sqrt{F}. \quad (58b)$$

Note that the amplitude of the shape resonances decreases with increasing  $\epsilon$  due to the factor  $f(\epsilon)$  in Eqs. (20) and (21).

### B. Phase shift $\delta_{n_1 m}(\epsilon, F)$

We turn next to the asymptotic phase shift  $\delta_{n_1 m}(\epsilon, F)$ , shown in Fig. 6 for  $n_1 = 0-5$ , with  $m = 0$  and  $F = 0.001$  a. u.  $= 5.1 \times 10^6$  V/cm. A large electric field has been chosen here to eliminate the higher  $(n_1, n_2, m)$  levels, in order to emphasize the effects of a nonzero  $F$ . Quasibound states correspond to the steps of  $\pi$ , as explained in Sec. III B, and are labeled by integral values of  $n_2 \geq 0$ . Each step is centered at

$$\delta_{n_1 m} / \pi = 2n_2 + 1 + \frac{1}{2}m, \quad (59)$$

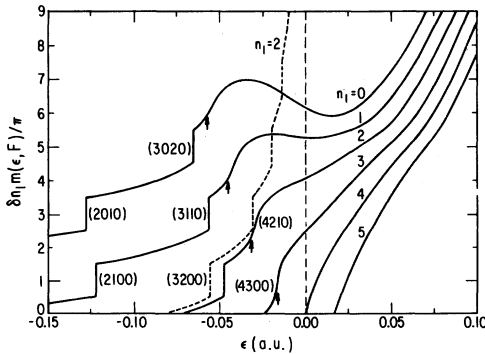


FIG. 6. Phase shift  $\delta_{n_1 m}(\epsilon, F)/\pi$  vs  $\epsilon$  for  $m = 0$ ,  $F = 0.001$  a. u., and  $n_1 = 0-5$  (solid curves). Quasibound levels, labeled by  $(n_1, n_2, m)$ , are centered at steps of  $\pi$  at  $\delta_{n_1 m} = (2n_2 + 1)\pi$ . Arrows indicate ionization thresholds  $\epsilon_c$ . Dashed curve shows phase shift for  $m = 0$ ,  $n_1 = 2$ ,  $F \rightarrow 0$ , with unperturbed Rydberg levels converging to  $\epsilon = 0$  threshold. Note Stark shift of  $n = 3$  states.  $\delta_{n_1 0} \xrightarrow{\epsilon \rightarrow \infty} (2\epsilon)^{3/2}/3F - \pi(n_1 + \frac{1}{2})$  [Eq. (60)].

in accordance with Eqs. (46) and (49), disregarding  $\delta_A$ , which is negligible for  $\epsilon < 0$ . [However, Eq. (59) becomes inaccurate as  $\epsilon$  approaches  $\epsilon_c$ ; see Sec. IV E.] Note (1) the steady increase of  $\delta_{n_1 m}$  between levels  $n_2$  and  $n_2 + 1$ , reflecting the behavior of  $\delta_{\text{out}}(\epsilon)$ , and (2) the total increase of  $2\pi$  per unit of  $n_2$ . The widths of all quasibound levels for  $n_1 = 0, 1$ , and  $2$  are too narrow to be resolved on the scale of Fig. 6, but the (4300) level appears as a shape resonance with width  $\Gamma = 0.0015$  a. u. centered at  $\epsilon = -0.0167$  a. u., just above the barrier top  $\epsilon_c = -0.0169$  a. u. [The (4210) shape resonance is less pronounced. See also Fig. 7.] There are no quasibound states for  $n_1 \geq 4$  for this value of  $F$ , as predicted by Eq. (57). Note that all the phase shifts in Fig. 6 rise more steeply just above the barrier top (indicated by arrows) as  $\chi_2(\eta)$  begins to oscillate. The closer  $\epsilon_c$  lies to the next quasibound level, the steeper will the rise be; if the well nearly supports another half-wavelength it will accumulate the remaining phase just above the barrier. This rise constitutes a shape resonance.

At high energies,  $\delta_{n_1 m}(\epsilon, F)$  is given by Eqs. (51), (35), and (B1); with  $\beta_2(\epsilon) = 1 - \beta_1(\epsilon)$  from Eq. (56), we have

$$\delta_{n_1 m}(\epsilon, F) = \frac{(2\epsilon)^{3/2}}{3F} - \pi(n_1 + \frac{1}{2}m + \frac{1}{4}) \\ + \pi Z\epsilon^{-1/2} + O(\alpha_1), \quad \epsilon \gg 0. \quad (60)$$

The divergence of  $\delta_{n_1 m}$  at large  $\epsilon$  shown by this equation derives from the increasing depth of the effective Coulomb well,  $-\beta_2(\epsilon)/\eta \sim -\epsilon^2/4F\eta$ , which accompanies the drop of  $\beta_1$  at fixed  $n_1$ . However, this divergence may be preceded by a maximum

and temporary decrease as shown in Fig. 6 for  $n_1 = 0$  and 1. Such a decrease with increasing  $\epsilon$  is familiar in all problems with an energy-independent potential; it occurs here whenever  $\epsilon > \epsilon_c$  and  $d\beta_2/d\epsilon$  is small.

The dashed curve of Fig. 6 shows the phase shift for  $n_1 = 2$ ,  $m = 0$ , and  $F \sim 0$ . The solid curve for  $n_1 = 2$  approaches the dashed curve increasingly as  $F$  decreases. For very low values of  $F$  the energy levels—marked by steps of the dashed curve—occur near their Rydberg values  $\epsilon = -\frac{1}{2}n^2$ . On the other hand, the barrier top  $\epsilon_c$  lowers as  $F$  increases, leaving an increasing number of levels in the classically ionized range, while the levels below  $\epsilon_c$  are slightly but increasingly displaced. For a field as large as that used in Fig. 6 ( $F = 0.001$ ) only two quasibound levels remain noticeable for  $n_1 = 2$ .

The divergence of the phase shift  $\delta_{n_1 m}$  of  $\chi_2(\eta)$  in the limit  $\epsilon \rightarrow \infty$  may at first seem surprising. Recall, however, that at  $\epsilon < 0$  even the zero-field hydrogenic functions  $\chi_1(\xi)$  or  $\chi_2(\eta)$  may have an arbitrarily large number of nodes,  $n_1$  or  $n_2$ . These quantum numbers gauge the amount of excitation in each mode. The total number of nodes  $n = n_1 + n_2 + m + 1$ , represents the excitation of the entire atom, which may be divided between  $\xi$  and  $\eta$  in varying proportions. Now we notice that the divergence of  $\delta_{n_1 m}$  is matched by a divergence of opposite sign in the phase shift of  $\chi_1(\xi)$  with respect to the corresponding Airy function in  $\xi$ ,  $\text{Di}(w(-\xi))$ , defined in Eq. (11). This phase shift is given by the difference of the quantized phase  $\pi(n_1 + 1)$  of  $\chi_1(\xi)$  and the phase  $-\delta_A$  of  $\text{Di}(w(-\xi))$ , given in Eq. (B2),

$$\int_0^{n_A} k_A(\xi') d\xi' + \frac{1}{4}\pi = \int_0^{2\epsilon/F} \left( \frac{1}{4}F\xi' - \frac{1}{2}\epsilon \right)^{1/2} d\xi' + \frac{1}{4}\pi$$

$$\xrightarrow{\epsilon \rightarrow \infty} \frac{(2\epsilon)^{3/2}}{3F} + \frac{1}{4}\pi.$$

The phase shift in  $\xi$  is then

$$\int_{-\xi_1}^{\xi_2} k(\xi') d\xi' - \int_0^{n_A} k_A(\xi') d\xi' - \frac{1}{4}\pi = \pi(n_1 + \frac{3}{4}) - \frac{(2\epsilon)^{3/2}}{3F},$$

$$\epsilon \gg 0 \quad (61)$$

which is large and *negative* due to the balancing of the Stark field by the *repulsive* Coulomb field of Eq. (56). The combined phase shift, defined as the sum of Eqs. (60) and (61), remains finite and equals  $-\frac{1}{2}(m-1)\pi + O(\epsilon^{-1/2})$ , which converges at  $\epsilon \rightarrow \infty$  to a *constant* phase shift due to the centrifugal barrier alone. Thus, the total phase shift of  $\psi$  does not diverge; rather, the presence of the Coulomb field *modifies* the Airy reference function through a transfer of excitation from the  $\xi$  coordinate to the  $\eta$  coordinate.

### C. Amplitude $A_{n_1 m}(\epsilon, F)$ ; partial cross sections

The amplitude factor  $A_{n_1 m}(\epsilon, F)$  of Eq. (12) is shown in Fig. 7 for the same values of  $n_1$ ,  $m$ , and  $F$  as those used in Fig. 6. We actually plot  $\ln A^{-1}(\epsilon)$  in order to represent as peaks the sharp minima of  $A_{n_1 m}$  at quasistationary levels, i.e., as they appear in the density of states (22),  $N_{\epsilon n_1 m}^F \propto A_{n_1 m}^{-2}$ . The positions  $\epsilon_{n_2}(n_1, m, F)$  and widths  $\Gamma_{n_2}(n_1, m, F)$  of these levels will be discussed in Sec. IV E. The heights of the peak maxima (indicated by dashed lines) follow from Eqs. (50), (38), and (44)–(46):

$$A_{n_1 0}^{-1}(\epsilon_{n_2}, F) = B_{n_1 0}^{1/2}(\epsilon_{n_2}) \cot \frac{1}{2}\theta$$

$$\approx 2\sqrt{2}e^\tau, \quad \epsilon < \epsilon_c. \quad (62)$$

Note that  $A_{n_1 0}^{-1}$  is proportional to  $d\delta_{n_1 0}/d\epsilon$  for  $\epsilon \approx \epsilon_{n_2}$  via the dispersion relation (47), as illustrated by Fig. 6 and 7.

Just above the barrier top for each  $n_1$  curve ( $\epsilon = \epsilon_c$ , arrows in Fig. 7) there is a modulation in the amplitude—the shape resonance due to the optical-type reflection discussed in Sec. III B. This “ringing” is stronger for the higher  $n_1$  states because their lower effective charge  $\beta_2$  at  $\epsilon_c$  sharpens the edge of the potential barrier. Far above the barrier, the factor  $R_{n_1 m}$  of Eq. (50) approaches unity. The amplitude,  $A_{n_1 m}(\epsilon \rightarrow \infty)$  reduces then to  $B_{n_1 m}^{-1/2}(\epsilon \rightarrow \infty)$  and depends only on the quantity

$$\beta_2/k \xrightarrow{\epsilon \rightarrow \infty} (2\epsilon)^{3/2}/16F$$

[see Eqs. (38) and (56)]. Since  $\beta_2/k > 0$  diverges also at  $\epsilon = 0$ , where  $k$  itself vanishes, we obtain the same form as  $B_{n_1 m}(\epsilon = 0)$ :

$$A_{n_1 m}^{-1}(\epsilon, F) = \frac{\sqrt{2}}{m!} |\beta_2|^{m/2} [1 + O(F\epsilon^{-3/2})], \quad \epsilon \gg 0 \quad (63)$$

$$\propto (\epsilon/\sqrt{F})^m,$$

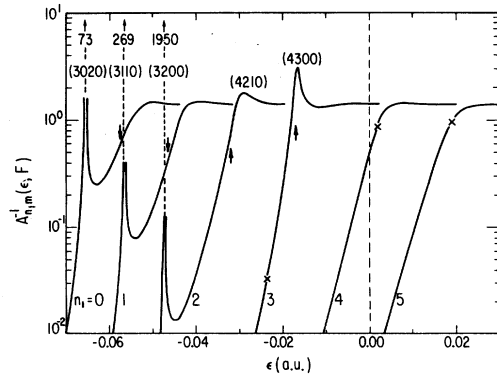


FIG. 7. Amplitude ratio  $A_{n_1 m}^{-1}(\epsilon, F) \propto \chi_2(\eta \sim 0)/\chi_2(\eta \sim \infty)$ , on log scale, vs  $\epsilon$  for  $m = 0$ ,  $F = 0.001$  (same as Figs. 3 and 6), and  $n_1 = 0-5$ . Peaks correspond to quasibound levels, below and above threshold  $\epsilon_c$  (arrows).  $\times$ :  $\beta_2(\epsilon, F; n_1, 0) = 0$ ;  $A_{n_1 0}^{-1} \xrightarrow{\epsilon \rightarrow \infty} \sqrt{2}$ .

which is independent of  $n_1$ . Although  $A_{n_1 m}^{-1}$  diverges as  $\epsilon^m$  in the limit of large  $\epsilon$  if  $m \neq 0$ , the density of states (22) eventually approaches zero due to the exponentially decreasing factor  $N_\epsilon \equiv \left\{ \int_0^\infty d\xi' [\chi_1(\xi')]^2 / \xi' \right\}^{-1}$  (see Sec. II, Fig. 3).

The above remarks on the large- $\epsilon$  behavior of  $A_{n_1 m}^{-1}(\epsilon, F)$  are similar to those on the large- $\epsilon$  behavior of  $\delta_{n_1 m}(\epsilon, F)$  discussed above. On the one hand, the zero-field threshold behavior of both  $\delta_{n_1 m}$  and  $A_{n_1 m}^{-1}$  is shifted from  $\epsilon=0$  to  $\epsilon=\infty$  when  $F \neq 0$  [Eqs. (60) and (63)]. On the other hand, when we consider the entire wave function (2) and the constraint (4), the divergences of  $\delta_{n_1 m}$  and  $A_{n_1 m}^{-1}$  are canceled by corresponding parameters of  $\chi_1(\xi)$ . Thus, in the limit  $\epsilon \rightarrow \infty$ , the Coulomb field will have no effect on  $\psi(\xi, \eta, \phi)$ ; there will only be centrifugal repulsion.

The shape resonances at  $\epsilon > 0$  in the density of states (22)—not due to quasibound levels—depend jointly on its two factors  $A_{n_1 m}^{-2}(\epsilon, F)$  and  $N_\epsilon$ , shown in Figs. 7 and 3 for  $m=0$ . In the range  $0 < \beta_1 < 1$ , and at  $\epsilon$  well above the barrier in  $\eta$ ,  $A_{n_1 m}^{-2}$  is given by (52a) or (52b), while  $N_\epsilon$  is given roughly by the same expressions with  $\beta_1$  in place of  $\beta_2$ . The order of magnitude of the density of states is then

$$N_{\epsilon_{n_1 m}}^F \sim \begin{cases} 1, & m=0 \\ \beta_1 \beta_2, & m=1 \end{cases}, \quad 0 < \beta_1 < 1. \quad (64a)$$

Note that  $N_{\epsilon_{n_1 0}}^F$  is flat, while  $N_{\epsilon_{n_1 1}}^F$  peaks parabolically. In fact,  $N_{\epsilon_{n_1 0}}^F$  and  $N_{\epsilon_{n_1 1}}^F$  for  $F=0$  and  $\epsilon < 0$  are given exactly by the expressions (64a) times a factor  $|\frac{1}{2}\epsilon|^{-1/2}$ . Thus, even in the presence of a Stark field,  $N_{\epsilon_{n_1 m}}^F$  closely resembles the density of states of the hydrogenic function for  $F=0$ , shifted in energy, as anticipated in Sec. IB.

At the upper (or lower) cutoff of any of these shape resonances, where  $\beta_1=0$  (or  $\beta_2=0$ ), this density of states drops to

$$N_{\epsilon_{n_1 m}}^F \sim \begin{cases} \frac{1}{2}(1 + e^{-2\tau/k})^{-1}, & m=0 \\ \frac{k}{2\pi}(1 - e^{-2\tau/k})^{-1}, & m=1 \end{cases}, \quad \beta_i=0 \quad (64b)$$

but does not actually vanish as would be indicated by (64a) for  $m=1$ . At energies beyond the shape resonance [ $\epsilon > \frac{1}{2}(3\pi n_1 F)^{2/3}$ , cf. Eq. (58a)], where  $\beta_1 < 0$  and  $A_{n_1 m}^{-2}$  is given in Eq. (54), the density of states decreases exponentially:

$$N_{\epsilon_{n_1 m}}^F \sim \begin{cases} e^{-2\tau|\beta_1|/k}, & m=0 \\ |\beta_1|\beta_2 e^{-2\tau|\beta_1|/k}, & m=1 \end{cases}, \quad \beta_1 < 0. \quad (64c)$$

Since  $\beta_1 = 1 - \beta_2 \approx -\epsilon^2/4F$  from Eq. (56), we see that  $N_{\epsilon_{n_1 m}}^F$  cuts off with increasing  $\epsilon$  as  $\exp(-\pi k^3/8F)$ . For  $m=0$  each partial density of states in Eq. (20) is further modulated by the factor  $(\beta_1 - \beta_2)^2$ . Hence the energy dependence of the  $m=0$  partial cross sections is parabolic with sharp cutoffs at  $\beta_1=0$ —

in contrast to the  $m=1$  partial cross sections, which essentially maintain their inverted parabolic shape (64a),  $\beta_1\beta_2$ . [See Figs. 1–3 of Ref. 11(a) and Fig. 11 of Ref. 4.]

#### D. Accuracy of $\delta_{n_1 m}$ and $A_{n_1 m}$ in the WKB approximation

The WKB expressions for  $\delta_{n_1 m}(\epsilon, F)$  and  $A_{n_1 m}(\epsilon, F)$  given in Sec. IIIB have been compared to the phase and amplitude of  $\chi_2(\eta \rightarrow \infty)$  from numerical integration of Eq. (3b). A large field strength was chosen,  $F=0.001$  a.u. ( $5.1 \times 10^6$  V/cm), for which the accuracy should be poorer than for laboratory field strengths. A Numerov procedure was used with blocks of varying step sizes to accommodate the qualitatively different behavior of  $\chi_2(\eta)$  in regions I, II, and III.

With a convergence of at least four significant figures for  $\delta_{n_1 m}$ , the error  $\Delta\delta_{n_1 m} = \delta_{n_1 m}^{\text{WKB}} - \delta_{n_1 m}^{\text{Num}}$  was found to have the following features:

- (1)  $\Delta\delta_{n_1 m}$  is negligible when  $\epsilon \ll \epsilon_c$ , even for  $n_1=0$ . For example, for  $n_1=0-3$  and  $m=0$  or 1,  $\Delta\delta_{n_1 m} < 0.002\pi$ .
- (2) There is a negative maximum in  $\Delta\delta_{n_1 m}$  at  $\epsilon \approx \epsilon_c$ . This error is smallest for  $n_1=0$ , where  $\beta_2 \gg \beta_{\text{crit}}$  and  $\Delta\delta_{n_1 m} \sim 0.007\pi$ . However,  $\Delta\delta_{n_1 m}$  increases with increasing  $n_1$  because, as anticipated,  $\beta_2(\epsilon_c)$  approaches  $\beta_{\text{crit}} \sim 0$ ; for  $n_1=3$ ,  $\Delta\delta_{n_1 m} \sim 0.018\pi$ .
- (3) If  $\beta_2 \approx \beta_{\text{crit}}$  and  $\epsilon > 0$ , there is a positive maximum error with  $\Delta\delta_{n_1 m} \lesssim 0.03\pi$ .
- (4) For  $\epsilon > 0$  with  $\beta_2 > \beta_{\text{crit}}$ , we have  $\Delta\delta_{n_1 m} \lesssim 0.006\pi$ .

The relative error in the amplitude,  $\Delta A_{n_1 m} = (A_{n_1 m}^{\text{WKB}}/A_{n_1 m}^{\text{Num}}) - 1$ , that is, the error in  $\ln A_{n_1 m}$ , is qualitatively linked to  $\Delta\delta_{n_1 m}$  by the dispersion relation  $\Delta A_{n_1 m} \propto d(\Delta\delta_{n_1 m})/d\epsilon$ ; in general,  $\Delta A_{n_1 m}(\epsilon \sim \epsilon_c)$  is about an order of magnitude larger than  $\Delta\delta_{n_1 m}$ . At  $\epsilon > \epsilon_c$ , for each  $n_1$ ,  $\Delta A_{n_1 m}$  is always smaller than 1% for  $F=0.001$ , except when  $\beta_2 \approx \beta_{\text{crit}}$ .

#### E. Quasibound states: Energy levels and widths

A quasistationary resonance of hydrogen is usually considered to be centered at the energy  $\epsilon_{n_2}^*(n_1, m, F)$  which marks the local extremum of  $R_{n_2 m}(\epsilon, F)$ ,<sup>8,11</sup> i.e., the inflection point of  $\gamma_{n_2 m}(\epsilon, F)$ . In Sec. IIIB it was suggested that  $\epsilon_{n_2}^*$  is well approximated by the energy  $\epsilon_{n_2}$  satisfying Eq. (46), i.e., such that

$$\delta_{i_n} + \frac{1}{2}\phi = \frac{1}{2}\pi(\text{mod } \pi) = \gamma_{n_1 m}.$$

The lowest levels, which correspond to large tunneling parameters (e.g., with  $\tau > 5$ ), have very sharp resonances. Therefore, the factor  $\tan\frac{1}{2}\theta(\tau)$  in Eqs. (43) and (44) remains nearly constant over the width of one of these levels and  $\epsilon_{n_2}$  essentially coincides with  $\epsilon_{n_2}^*$  for given  $n_1, m, F$ . However, for a resonance approaching the barrier top,  $\epsilon_{n_2}$  will

lie increasingly higher than the actual level  $\epsilon_{n_2}^*$ . If the resonance occurs near or above  $\epsilon_c$ ,  $|\tau|$  is small and  $\epsilon_{n_2}$  may only serve as a first guess to  $\epsilon_{n_2}^*$ .

The full width  $\Gamma_{n_2}(n_1, m, F)$  (in a.u.) of a quasi-stationary resonance is obtained by assuming a Lorentzian profile for the intensity of each  $n_2$  level

$$R_{n_1 m}^{-2}(\epsilon, F) = \frac{R_{n_1 m}^{-2}(\epsilon_{n_2}, F)}{(\epsilon - \epsilon_{n_2})^2 + (\frac{1}{2}\Gamma_{n_2})^2} \quad (65)$$

and a concomitant arctangent form for the phase,

$$\gamma_{n_1 m} - \pi(2n_2 + 1 + \frac{1}{2}m) = \tan^{-1}[(\epsilon - \epsilon_{n_2})/\frac{1}{2}\Gamma_{n_2}]. \quad (66)$$

The width is then

$$\Gamma_{n_2} = 2 \left( \tan^2 \frac{1}{2} \theta \frac{d(\delta_{1n} + \frac{1}{2} \phi)}{d\epsilon} \right)_{\epsilon = \epsilon_{n_2}} \quad (67)$$

if we again assume that  $\tan \frac{1}{2} \theta(\tau) \approx \frac{1}{2} e^{-\tau}$  is approximately constant over the energy range  $\epsilon_{n_2} \pm \frac{1}{2} \Gamma_{n_2}$ . The lifetime of an  $(n_1 n_2 m)$  state for fixed  $n_1, m$ , and  $F$  is simply  $T_{n_1 n_2 m} = \Gamma_{n_2}^{-1}$  a.u.  $= (\hbar^3/m e^4) \Gamma_{n_2}^{-1}$  sec. Generally, the value of  $\epsilon_{n_2}$  from Eq. (46) is more accurate than the corresponding  $\Gamma_{n_2}$  by about one significant figure, but  $\Gamma_{n_2}$  is always at least of the correct order of magnitude, even for the highest  $n_2$  states.<sup>30</sup>

*Note added in proof.* A recent paper by V. D. Kondratovich and V. N. Ostrovskii, Zh. Eksp. Teor. Fiz. 79, 395 (1980) [Sov. Phys.—JETP 52, 198 (1981)], has obtained substantially equivalent results for the photoionization cross section in a more compact mathematical presentation initiated by G. F. Drukarev.

#### ACKNOWLEDGMENTS

I would like to express my deep appreciation to Professor U. Fano for his continuing support and guidance, and especially for his extensive help with the manuscript. I am also indebted to Dr. K. T. Lu for encouraging this work and to several colleagues for many useful discussions. This research was supported by the U. S. Department of Energy, Office of Basic Energy Sciences. Presented to the Department of Physics, The University of Chicago, in partial fulfillment of the requirements for the Ph.D. degree.

#### APPENDIX A: EXTENDED WKB TREATMENT

Miller and Good's extension of the WKB method to deal with zeroes of the kinetic energy<sup>5(a)</sup> is presented here through examples of increasing complexity. The usual WKB method relies on the near constancy of the wave number  $k(\eta)$  in the equation

$$\left( \frac{d^2}{d\eta^2} + k^2(\eta) \right) \chi(\eta) = 0. \quad (A1)$$

The condition  $k(\eta) \sim \text{const}$  suggests representing  $\chi(\eta)$  as a trigonometric function of a phase  $x$  defined by

$$\int_a^x dx' \sim \int_b^\eta k(\eta') d\eta'. \quad (A2)$$

The first derivative  $dk/d\eta$  is taken into account through the familiar amplitude factor  $[k(\eta)]^{-1/2}$  which ensures normalization per unit energy. The method breaks down at any node of  $k^2(\eta)$ .

The presence of a single node  $b$  is taken into account by replacing locally the WKB trigonometric function by an Airy function, a solution of (A1) with  $k^2(\eta)$  linear in  $\eta$ . The argument  $x(\eta)$  of the Airy function is now given through the relation

$$\int_a^{x(\eta)} (x' - \alpha)^{1/2} dx' = \int_b^\eta k(\eta') d\eta'. \quad (A3)$$

The first derivative of  $k(\eta)$  is taken into account through renormalization of the Airy function by the factor

$$(x - \alpha)^{1/4} [k(\eta)]^{-1/2}, \quad (A4)$$

which remains finite at the zero of  $k(\eta)$ .<sup>31</sup> Higher derivatives are dropped again and the asymptotic form of the Airy function reduces to the WKB expression, plus the extra phase  $\pi/4$  as usually given in the connection formulas. This is essentially the procedure followed by Lanczos.<sup>14</sup>

The presence of a pair of nodes,  $a$  and  $b$  (real or complex conjugate, as in Fig. 4), is taken into account by replacing the WKB trigonometric function, over a range including the nodes, by a parabolic cylinder function which obeys the equation

$$\left( \frac{d^2}{dx^2} + (\frac{1}{4}x^2 - \alpha) \right) y(x) = 0. \quad (A5)$$

The argument  $x(\eta)$  is given by the transformation analogous to (A3),

$$\int_{-2\sqrt{\alpha}}^x (\frac{1}{4}x'^2 - \alpha)^{1/2} dx' = \int_b^\eta k(\eta') d\eta', \quad (A6)$$

where  $b$  is the node of  $k(\eta)$  such that  $\arg(a - b) = 0$  (for  $a, b$  real) or  $-\frac{1}{2}\pi$  (for  $a = b^*$ ). The value of  $\alpha$  is set by matching  $\eta = a$  to  $x = 2\sqrt{\alpha}$ ,

$$\begin{aligned} \int_b^a k(\eta') d\eta' &= \int_{-2\sqrt{\alpha}}^{2\sqrt{\alpha}} (\frac{1}{4}x'^2 - \alpha)^{1/2} dx' \\ &= i\pi\alpha \equiv i\tau, \end{aligned} \quad (A7)$$

with the tunneling integral  $\tau$  introduced in Eq. (31). The renormalization factor of the parabolic cylinder function is now

$$(\frac{1}{4}x^2 - \alpha)^{1/4} [k(\eta)]^{-1/2} \quad (A8)$$

and higher derivatives of  $k(\eta)$  are once more not included. The asymptotic form of the renormalized parabolic cylinder function at large  $|x|$  re-

duces again to the usual WKB expression but with the desired phase corrections, which are described below.

As parabolic cylinder basis functions we choose the standing wave solutions which are *even* [ $y_1(x)$ ] and *odd* [ $y_2(x)$ ] with respect to  $x=0$ . Their asymptotic forms are given through Eqs. (19.17.1), (19.17.8), and (19.21.2-3) on pp. 692-3 of Ref. 16:

$$y_1(x) \xrightarrow{|x| \rightarrow \infty} \left| \frac{1}{2}x \right|^{-1/2} \sin[f(x, \alpha) + \frac{1}{4}\pi - \frac{1}{2}\theta]$$

and

$$y_2(x) \xrightarrow{|x| \rightarrow \infty} \pm \left| \frac{1}{2}x \right|^{-1/2} \sin[f(x, \alpha) + \frac{1}{4}\pi + \frac{1}{2}\theta], \quad x \geq 0 \quad (\text{A9})$$

where

$$f(x, \alpha) = \frac{1}{4}x^2 - \alpha \ln|x| + \frac{1}{2} \arg\Gamma\left(\frac{1}{2} + i\alpha\right) \quad (\text{A10})$$

and

$$\theta \equiv \tan^{-1}(e^{-\tau\alpha}), \quad 0 < \theta < \frac{1}{2}\pi \quad (\text{A11})$$

$\alpha$  being defined by (A5) and (A7). For our purposes, the phase function (A10) will be compared with the asymptotic form of the phase integral (A6),

$$\begin{aligned} \int_{-x}^{-2\sqrt{\alpha}} \left(\frac{1}{4}x'^2 - \alpha\right)^{1/2} dx' &= \int_{2\sqrt{\alpha}}^x \left(\frac{1}{4}x'^2 - \alpha\right)^{1/2} dx' \\ &= \frac{1}{2}x \left(\frac{1}{4}x^2 - \alpha\right)^{1/2} - \alpha \ln\left[\frac{1}{2}x + \left(\frac{1}{4}x^2 - \alpha\right)^{1/2}\right] + \frac{1}{2}\alpha \ln|\alpha| \\ &\xrightarrow{|x| \rightarrow \infty} \frac{1}{4}x^2 - \alpha \ln|x| - \frac{1}{2}\alpha(1 - \ln|\alpha|). \end{aligned}$$

With these substitutions Eqs. (A9) become

$$\begin{aligned} y_1(x) &\xrightarrow{|x| \rightarrow \infty} \left| \frac{1}{2}x \right|^{-1/2} \sin\left(\int_{2\sqrt{\alpha}}^x \left(\frac{1}{4}x'^2 - \alpha\right)^{1/2} dx' + \frac{1}{4}\pi + \frac{1}{2}\phi - \frac{1}{2}\theta\right), \\ y_2(x) &\xrightarrow{|x| \rightarrow \infty} \pm \left| \frac{1}{2}x \right|^{-1/2} \sin\left(\int_{2\sqrt{\alpha}}^x \left(\frac{1}{4}x'^2 - \alpha\right)^{1/2} dx' + \frac{1}{4}\pi + \frac{1}{2}\phi + \frac{1}{2}\theta\right), \quad x \geq 0 \end{aligned} \quad (\text{A12})$$

where

$$\phi(\alpha) = \arg\Gamma\left(\frac{1}{2} + i\alpha\right) + \alpha(1 - \ln|\alpha|), \quad \alpha = \tau/\pi \quad (\text{A13})$$

indicates the correction term introduced as Eq. (42).

To derive the desired connection formula for  $\chi_2(\eta)$ , we start to the left of the barrier with a general WKB solution of Eq. (A1),

$$\chi_L(\eta) = R_L k^{-1/2}(\eta) \cos\left(\int_{\eta}^b k(\eta') d\eta' + \frac{1}{4}\pi - \delta_L\right), \quad \eta \ll \text{Re}(b) \quad (\text{A14})$$

where the phase  $\delta_L$  and amplitude  $R_L$  are initially arbitrary. We will obtain a solution to the right of the barrier of the form

$$\chi_R(\eta) = R_R k^{-1/2}(\eta) \sin\left(\int_a^{\eta} k(\eta') d\eta' + \frac{1}{4}\pi + \delta_R\right), \quad \eta \gg \text{Re}(a). \quad (\text{A15})$$

With the above notation, the solution (A14) may now be expressed through the basis functions (A12), using Eqs. (A6) and (A7):

$$\chi_L(\eta) = \left(\frac{\frac{1}{2}|x|}{k(\eta)}\right)^{1/2} \frac{R_L}{\sin\theta} [\cos(\delta_L + \frac{1}{2}\phi + \frac{1}{2}\theta)y_1(x) - \cos(\delta_L + \frac{1}{2}\phi - \frac{1}{2}\theta)|y_2(x)|]. \quad (\text{A16})$$

To obtain  $\chi_R(\eta)$ , we evaluate Eq. (A16) at  $x \gg 0$  by merely flipping the sign of the odd function:

$$\begin{aligned} \chi_R(\eta) &= \left(\frac{\frac{1}{2}x}{k(\eta)}\right)^{1/2} \frac{R_L}{\sin\theta} [\cos(\delta_L + \frac{1}{2}\phi + \frac{1}{2}\theta)y_1(x) + \cos(\delta_L + \frac{1}{2}\phi - \frac{1}{2}\theta)y_2(x)] \\ &= k^{-1/2}(\eta) R_L \frac{2 \cos^2 \frac{1}{2}\theta \cos(\delta_L + \frac{1}{2}\phi)}{\sin\theta} \left[ \sin\left(\int_{2\sqrt{\alpha}}^x \left(\frac{1}{4}x'^2 - \alpha\right)^{1/2} dx' + \frac{1}{4}\pi + \frac{1}{2}\phi\right) \right. \\ &\quad \left. + \tan^2\left(\frac{1}{2}\theta\right) \tan(\delta_L + \frac{1}{2}\phi) \cos(\dots) \right] \\ &= k^{-1/2}(\eta) R_L \frac{\cot \frac{1}{2}\theta \cos(\delta_L + \frac{1}{2}\phi)}{\cos\gamma} \sin\left(\int_{2\sqrt{\alpha}}^x \left(\frac{1}{4}x'^2 - \alpha\right)^{1/2} dx' + \frac{1}{4}\pi + \frac{1}{2}\phi + \gamma\right), \end{aligned} \quad (\text{A17})$$

where

$$\tan\gamma \equiv \tan^2(\frac{1}{2}\theta)\tan(\delta_L + \frac{1}{2}\phi). \quad (\text{A18})$$

Direct comparison of Eqs. (A15) and (A17) [again using Eq. (A6)] furnishes the phase

$$\delta_R = \frac{1}{2}\phi + \gamma \quad (\text{A19})$$

and amplitude

$$R_R = R_L \cot(\frac{1}{2}\theta)\cos(\delta_L + \frac{1}{2}\phi)\sec\gamma. \quad (\text{A20})$$

The connection formula implied by Eqs. (A19) and (A20) is expressed compactly by

$$\sin\frac{1}{2}\theta \cos\left(\int_a^b k(\eta')d\eta' + \frac{1}{4}\pi + \frac{1}{2}\phi\right) \leftrightarrow \cos\frac{1}{2}\theta \sin\left(\int_a^n k(\eta')d\eta' + \frac{1}{4}\pi + \frac{1}{2}\phi\right) \quad (\text{A21a})$$

and the companion formula

$$\cos\frac{1}{2}\theta \sin\left(\int_a^b k(\eta')d\eta' + \frac{1}{4}\pi + \frac{1}{2}\phi\right) \leftrightarrow \sin\frac{1}{2}\theta \cos\left(\int_a^n k(\eta')d\eta' + \frac{1}{4}\pi + \frac{1}{2}\phi\right). \quad (\text{A21b})$$

#### APPENDIX B: THE AIRY PHASE SHIFT

We specify here the branch of the tangent in Eq. (9) which defines the Airy correction  $-\delta_A$ . When  $w(\eta) < 0$ , the Airy functions<sup>16</sup>  $\text{Ai}(w)$  and  $\text{Bi}(w)$  vanish and diverge, respectively, as  $\exp(\mp \frac{2}{3}|w|^{3/2})$ . Hence, this correction is positive and very small at negative energies, increasing as  $\epsilon$  approaches zero, where it reaches the value  $\pi/6$ . At  $\epsilon > 0$   $\text{Ai}(w)$  and  $\text{Bi}(w)$  start oscillating in the region  $w < w_0 \equiv w(\eta=0) = (2/F^2)^{1/3}\epsilon$  [cf. Eq. (7)] and  $-\delta_A$  represents the total accumulation of phase of  $\text{Ai}(w)$  from  $w = -\infty$  to  $w = w_0$ . Stipulating here that  $-\frac{1}{2}\pi \leq \tan^{-1}(\dots) < \frac{1}{2}\pi$ , we have then

$$-\delta_A(\epsilon, F) = \tan^{-1}\left(\frac{\text{Ai}(w_0)}{\text{Bi}(w_0)}\right) + \pi N_{\text{Bi}} \quad (\text{B1})$$

$$\xrightarrow{\epsilon \gg 0} \frac{(2\epsilon)^{3/2}}{3F} + \frac{1}{4}\pi, \quad (\text{B2})$$

where  $N_{\text{Bi}}$  is the number of nodes of  $\text{Bi}(w \leq w_0)$ .

#### APPENDIX C: ELLIPTIC INTEGRALS AND PHASE CORRECTION

The WKB phase integral introduced in Eq. (25) for obtaining the eigenvalues  $\beta_1(\epsilon, F; n_1, m)$  may be

$$F^{-1/2}(a-c)^{-1/2}\left(\frac{2}{3}(\epsilon c + 4\beta_1)K(\kappa) + \frac{2}{3}\epsilon(a-c)E(\kappa) - \frac{m^2}{a}\Pi(\nu \backslash \kappa)\right) + \Delta\sigma_m = \pi(n_1 + \frac{1}{2}), \quad (\text{C3})$$

with the correction  $\Delta\sigma_m$  discussed below.

In the special case  $m=0$ , the canonical integral  $\Pi(\nu \backslash \kappa)$  drops out of Eq. (C3). One of the three roots of the polynomial then vanishes identically, namely,  $b=0$  for  $\beta_1 > 0$  and  $c=0$  for  $\beta_1 < 0$ , while the two nonzero roots are

reduced to a complete elliptic integral when expressed in terms of all three roots of its integrand [cf. Eq. (28)]:

$$2F^{-1/2} \int_{\xi_1}^{\xi_2} \left(-\frac{m^2}{4\xi'^2} + \frac{\beta_1}{\xi'} + \frac{1}{2}\epsilon - \frac{1}{4}F\xi'\right)^{1/2} d\xi' \\ = \int_b^a [(a-\xi')(\xi'-b)(\xi'-c)]^{1/2} \frac{d\xi'}{\xi'}, \quad (\text{C1})$$

where

$$c < 0 \leq b = \xi_1 \leq \xi' \leq a = \xi_2.$$

This integral can be expressed in turn as a linear combination of the three canonical forms denoted in Refs. 26 and 32 as  $K(\kappa)$ ,  $E(\kappa)$ , and  $\Pi(\nu \backslash \kappa)$ , where script letters denote the corresponding symbols in these references and

$$\kappa^2 = \frac{a-b}{a-c} < \nu = \frac{a-b}{a} < 1. \quad (\text{C2})$$

Note that  $\kappa^2$  vanishes when  $\epsilon$  drops to the bottom of the potential well and rises instead towards unity with increasing  $\epsilon$ . Now the quantization equation (25) takes the form

$$[\epsilon \pm (\epsilon^2 + 4\beta_1 F)^{1/2}]/F.$$

The complete elliptic integrals  $K$ ,  $E$ , and  $\Pi$  can be calculated by an extremely simple and quickly convergent iterative method due to Gauss, the "process of the arithmetic-geometric mean," de-

scribed on p. 598 of Ref. 32. One can, for example, correctly obtain  $K$  and  $E$  to ten decimal places with five or fewer iterations for  $\kappa < 0.99999$ . Series expansions in the variables  $\kappa^2$  or  $1 - \kappa^2$  are convenient when  $\kappa^2$  approaches its limiting values of 0 or 1.

The calculations of  $\beta_1(\epsilon, F; n_1, m)$  may now proceed as follows, for given  $m$  and  $F$ : (i) over a given range of energies, choose a mesh size for  $\epsilon$ ; (ii) for a single  $\epsilon$ , determine the value of  $\beta_1$  for which  $b = a$  and  $\kappa = 0$ , i.e., such that the minimum of the potential well  $U(\xi) = \frac{1}{4}m^2/\xi^2 - \beta_1/\xi + \frac{1}{4}F\xi$  coincides with the energy  $\frac{1}{2}\epsilon$  (this involves solving a cubic equation); (iii) increase  $\beta_1$  and calculate  $n_1(\beta_1, \epsilon)$  from (C3) for two or more values of  $\beta_1$ ; (iv) from the last two  $n_1(\beta_1, \epsilon)$  points extrapolate and/or interpolate this function to a desired value of  $n_1 = 0, 1, 2, \dots$  to determine a next guess for  $\beta_1(\epsilon, F, n_1, m)$ ; (v) iterate step (iv) until  $\beta_1(\epsilon, F; n_1, m)$  is interpolated to a specified accuracy; (vi) extrapolate to the next integer  $n_1$  [as in step (iv)] and repeat the above iteration; (vii) repeat steps (ii)–(vi) for the entire mesh of  $\epsilon$  values; (viii) plot all the values of  $\beta_1$  thus obtained against  $\epsilon$ , interpolating in  $\epsilon$  as needed along each curve with constant  $n_1$ .

Here we note an appreciable though small correction to the WKB phase integral for positive-energy Coulomb wave functions. It is well known that, for  $\epsilon < 0$ , the WKB integral in Eq. (24) for the accumulated phase across the entire Coulomb well gives precisely the relation

$$\pi[(-2\epsilon)^{-1/2}\beta_1 - \frac{1}{2}m] = \pi(n_1 + \frac{1}{2}),$$

which is required to truncate the confluent hypergeometric series for the exact Coulomb wave function. (In fact, Langer sought to elucidate this circumstance.) For  $\epsilon > 0$ , evaluation of the WKB phase integral yields the asymptotic form

$$\chi_1(\xi) \propto \sin[\frac{1}{2}k\xi + (\beta_1/k) \ln k\xi - \frac{1}{4}m\pi + \frac{1}{4}\pi + \sigma_m^{\text{WKB}}], \quad (\text{C4})$$

with the phase shift

$$\begin{aligned} \sigma_m^{\text{WKB}} &= \alpha(1 - \ln|\alpha|) - \frac{1}{2}\alpha \ln[1 + (\frac{1}{2}m/\alpha)^2] \\ &\mp \frac{1}{2}m \sin^{-1}[1 + (\frac{1}{2}m/\alpha)^2]^{-1/2} + O(\xi^{-1}), \\ \alpha &= \beta_1/k \geq 0. \end{aligned} \quad (\text{C5})$$

The analytic expression for the regular Coulomb function<sup>13,27</sup> has the same asymptotic form as (C4), except the phase shift  $\sigma_m^{\text{WKB}}$  is replaced by

$$\sigma_m^{\text{Coul}} = \arg\Gamma(\frac{1}{2} + \frac{1}{2}m - i\beta_1/k). \quad (\text{C6})$$

Hence for positive energies we must add to the WKB phase integral the small correction

$$\Delta\sigma_m = \sigma_m^{\text{Coul}} - \sigma_m^{\text{WKB}}; \quad (\text{C7})$$

$\Delta\sigma_m$  is odd in  $\alpha$  and vanishes in both limits  $\alpha = 0$  and  $\alpha \rightarrow \infty$ . At small energies it equals  $-k/24\beta_1$  and has the following peak values:

$$\begin{aligned} m &= 0, 1, 2; \\ \alpha_{\text{max}} &= 0.178, 0.626, 1.079; \end{aligned} \quad (\text{C8})$$

$$\Delta\sigma_{\text{max}}/\pi = 0.0479, 0.0120, 0.0064.$$

The correction will obviously apply also in the presence of the Stark field when  $\epsilon > 0$ . It will be ignored in many formulas for notational simplicity, but it should actually be taken into account; cf. Eqs. (24), (25), (35), (40), (43), (44), (48), and (51).

#### APPENDIX D: ANALYSIS OF $\int_{-\infty}^{\infty} k(\eta') d\eta'$

We wish to isolate the real and imaginary pieces of the integrals in Eq. (29). Since the loop integral around either contour of Fig. 4 vanishes, we must have

$$(\text{Re and Im}) \int_{-\infty}^{\infty} \delta k(\eta') d\eta' = 0. \quad (\text{D1})$$

With the definitions (30)–(31') of Sec. IIIA, the fundamental relationships (33),  $\delta_{\text{out}} - \delta_{\text{in}} = \frac{1}{2}m\pi$ , and (34),  $\tau = \tau'$ , will be seen to hold for both cases  $\epsilon < \epsilon_c$  and  $\epsilon > \epsilon_c$ .

Below the barrier,  $\epsilon < \epsilon_c$ . Consider first the case  $\epsilon < \epsilon_c$ , where all three turning points of  $k(\eta)$  are real,  $0 \leq c < b < a$  [see Fig. 4(a)]. The branch cuts of  $k(\eta)$  extend over the ranges of the real axis  $-\infty < \eta < c$  and  $b < \eta < a$ . As  $\eta$  decreases from  $+\infty$  to  $-\infty$ , just above the real axis, the phase of  $[(\eta - a)(\eta - b)(\eta - c)]^{1/2}$  in Eq. (28) increases by  $\frac{1}{2}\pi$  upon passing each branch point. On the positive imaginary side of the branch cuts, along the real axis, the phase  $\varphi(\eta) = \arg\{[(\eta - a)(\eta - b)(\eta - c)]^{1/2}/\eta\}$  is then

$$\varphi(\eta) = \begin{cases} 0, & \eta > a \\ \frac{1}{2}\pi, & b < \eta < a \\ \pi, & c < \eta < b \\ \frac{3}{2}\pi, & 0 < \eta < c \\ \frac{1}{2}\pi, & \eta < 0, \quad \epsilon < \epsilon_c. \end{cases}$$

Similarly,

$$\arg[\eta - \eta_A]^{1/2} = \begin{cases} 0, & \eta > \eta_A \\ \frac{1}{2}\pi, & \eta < \eta_A. \end{cases}$$

The first and third (second and fourth) terms on the rhs of Eq. (29) are therefore purely real (imaginary); explicitly indicating the phase factors of  $k(\eta)$ ,  $1, i, i^2 = -1$  and  $i^3 = -i$ , Eq. (29) becomes

$$\int_{-\infty}^{\infty} \delta k(\eta') d\eta' = \operatorname{Re} \left( \int_a^{\infty} k(\eta') d\eta' - \int_{\eta_A}^{\infty} k_A(\eta') d\eta' \right) + i \operatorname{Im} \int_b^a k(\eta') d\eta' \\ - \left| \operatorname{Re} \int_c^b k(\eta') d\eta' \right| - i \operatorname{Im} \left( -\mathcal{P} \int_{-\infty}^c k(\eta') d\eta' + \int_{-\infty}^{\eta_A} k_A(\eta') d\eta' \right) - \frac{1}{2} m \pi. \quad (\text{D2})$$

Now Eq. (D1) gives Eqs. (33) and (34) directly.

Above the barrier,  $\epsilon > \epsilon_c$ . These results apply as well to the case  $\epsilon > \epsilon_c$ , where the turning points  $a$  and  $b$  become complex conjugates,  $b = a^* = b_1 + i a_1$  [see Fig. 4(b)]. The branch cut between  $a$  and  $b$  now parallels the imaginary axis, crossing the real axis at  $\eta = b_1$ . The contour is deformed so that it still follows a path from one turning point to the next without enclosing any poles or crossing any branch cuts. To recover Eqs. (33) and (34), we again note the phase of  $k(\eta)$  and the pieces of Eq. (29), which now contain both on- and off-axis integrals:

$$\int_{-\infty}^{\infty} \delta k(\eta') d\eta' = \left( \int_{b_1}^{\infty} k(\eta') d\eta' + \int_a^{b_1} k(\eta') i |d\eta'| - \int_{\eta_A}^{\infty} k_A(\eta') d\eta' \right) + \int_b^a k(\eta') i |d\eta'| \\ + \left( \int_{b_1}^b k(\eta') i |d\eta'| + \int_c^{b_1} k(\eta') d\eta' \right) + \left( \int_{-\infty}^c k(\eta') d\eta' - \int_{-\infty}^{\eta_A} k_A(\eta') d\eta' \right). \quad (\text{D3})$$

Along the real axis we find

$$\varphi(\eta) = \begin{cases} 0, & \eta \geq b_1 + \rho \\ \pi, & c < \eta \leq b_1 - \rho \\ \frac{3}{2}\pi, & 0 < \eta < c \\ \frac{1}{2}\pi, & \eta < 0, \quad \epsilon > \epsilon_c \end{cases}$$

avoiding the branch cut at  $\eta = b_1$  by the infinitesimal  $\rho \rightarrow 0^+$ . Defining  $\theta_b = \varphi(\eta = b) = -\varphi(\eta = a) = \frac{1}{2} \tan^{-1}[a_1/(b_1 - c)] + \frac{1}{4}\pi < \frac{3}{2}\pi$ , along the three off-axis segments of the contour the phase of  $k(\eta)$  is now

$$-\theta_b < \varphi \leq 0, \quad a + \rho \leq \eta \leq b_1 + \rho, \\ -\theta_b < \varphi < \theta_b, \quad a + \rho \leq \eta \leq b + \rho, \\ \pi \geq \varphi > \pi - \theta_b, \quad b_1 - \rho \leq \eta \leq b - \rho.$$

Now the real and imaginary parts of the integrals

along these segments are given in the limit  $\rho \rightarrow 0$  in terms of real numbers  $X, Y > 0$  by

$$\int_{a+\rho}^{b_1+\rho} |k(\eta')| e^{i\varphi} i |d\eta'| = X + iY, \\ \int_{b+\rho}^{a+\rho} |k(\eta')| e^{i\varphi} i |d\eta'| = - \int_{a+\rho}^{b+\rho} (\dots) = -2iY, \quad (\text{D4}) \\ \int_{b_1-\rho}^{b-\rho} |k(\eta')| e^{i\varphi} i |d\eta'| = X - iY;$$

note that the integral from  $b - \rho$  to  $b + \rho$ , rounding the branch point  $b$ , vanishes as  $\rho \rightarrow 0$ . Thus, the second and fourth bracketed terms on the rhs of Eq. (D3) are again purely imaginary, as in Eq. (D2) for  $\epsilon < \epsilon_c$ , but  $\tau$  is now *negative*; also, the sum of the first and third terms is again purely real. Through Eq. (D1) and the definitions of Sec. IIIA, we again have Eqs. (33) and (34).

<sup>1</sup>(a) For studies on Rb, see R. R. Freeman, N. P. Economou, G. C. Bjorklund, and K. T. Lu, Phys. Rev. Lett. **41**, 1463 (1978); R. R. Freeman and N. P. Economou, Phys. Rev. A **20**, 2356 (1979); (b) For rare-gas atoms see, B. E. Cole, J. W. Cooper, and E. B. Saloman, Phys. Rev. Lett. **45**, 887 (1980); (c) For alkaline earths see, W. Sandner, T. F. Gallagher, and K. A. Safinya, in *Abstracts of the 7th International Conference on Atomic Physics* (M.I.T., Cambridge, 1980), p. 199(A); H. Metcalf (unpublished).  
<sup>2</sup>A. R. P. Rau, J. Phys. B **12**, L193 (1979); A. R. P. Rau and K. T. Lu, Phys. Rev. A **21**, 1057 (1980).  
<sup>3</sup>(a) M. L. Zimmerman, M. G. Littman, M. M. Kash, and D. Kleppner, Phys. Rev. A **20**, 2251 (1979); M. G. Littman, M. M. Kash, and D. Kleppner, Phys. Rev. Lett. **41**, 103 (1978); (b) W. E. Cooke and T. F. Gallagher, Phys. Rev. A **17**, 1226 (1978); (c) S. Feneuille,

S. Liberman, J. Pinard, and A. Taleb, Phys. Rev. Lett. **42**, 1404 (1979).

<sup>4</sup>D. F. Blossey, Phys. Rev. B **2**, 3976 (1970).

<sup>5</sup>(a) S. C. Miller and R. H. Good, Jr., Phys. Rev. **91**, 174 (1953); (b) M. S. Child, J. Mol. Spectrosc. **53**, 280 (1974).

<sup>6</sup>H. J. Silverstone, Phys. Rev. A **18**, 1853 (1978); P. M. Koch, Phys. Rev. Lett. **41**, 99 (1978).

<sup>7</sup>R. J. Damburg and V. V. Kolosov, J. Phys. B **9**, 3149 (1976); Phys. Lett. **61A**, 233 (1977); J. Phys. B **11**, 1921 (1978); **12**, 2637 (1979); in *Invited Papers and Progress Reports of the Eleventh ICPEAC, Kyoto, 1979*, edited by K. Takayanagi and N. Oda (North-Holland, Amsterdam, 1980), p. 741.

<sup>8</sup>M. H. Rice and R. H. Good, Jr., J. Opt. Soc. Am. **52**, 239 (1962).

<sup>9</sup>D. S. Bailey, J. R. Hiskes, and A. C. Riviere, Nucl.

- Fus. 5, 41 (1965).
- <sup>10</sup>S. Liberman and J. Pinard, *Phys. Rev. A* 20, 507 (1979); E. Luc-Koenig, S. Liberman, and J. Pinard, *ibid.* 20, 519 (1979); see also S. Feneuille and P. Jacquinet, in *Atomic Physics 6*, edited by R. J. Damburg (Plenum, New York, 1979), p. 626 and references therein.
- <sup>11</sup>(a) E. Luc-Koenig and A. Bachelier, *Phys. Rev. Lett.* 43, 921 (1979); (b) *J. Phys. B* 13, 1743 (1980); (c) *ibid.* 13, 1769 (1980).
- <sup>12</sup>U. Fano, *Phys. Rev. A* 24, 619 (1981).
- <sup>13</sup>C. Greene, U. Fano, and G. Strinati, *Phys. Rev. A* 19, 1485 (1979); see also U. Fano, *Comments At. Mol. Phys.* X, 223 (1981).
- <sup>14</sup>C. Lanczos, *Z. Phys.* 65, 431 (1930).
- <sup>15</sup>L. D. Landau and E. M. Lifshitz, *Quantum Mechanics (Non-Relativistic Theory)*, 3rd ed. (Pergamon, Oxford, 1976), p. 62f and Sec. 77.
- <sup>16</sup>M. Abramowitz and I. A. Stegun, *Handbook of Mathematical Functions* (Dover, New York, 1970), Chap. 10.4.
- <sup>17</sup>Strictly speaking, the wave functions in Eqs. (8) and (39) are *not* normalized per unit  $\epsilon$  but rather per unit  $\frac{1}{4}\epsilon$ : although  $Ci(\eta)$  and  $\chi_2^{1/2}(\eta)$  each have the *form* of an energy-normalized solution—with the factor  $[2/\pi k(\eta)]^{1/2}$ —their wave numbers depend on  $\frac{1}{2}\epsilon$  rather than  $2\epsilon$ . The coefficient  $A_{n_1 m}$ , resulting from the energy-independent normalization of  $\chi_2(\eta)$  near  $\eta=0$ , enters instead into the energy normalization of the *entire* wave function. [See Sec. IB, Eq. (22) and Ref. 27 below.]
- <sup>18</sup>See, e.g., L. J. Schiff, *Quantum Mechanics*, 3rd ed. (McGraw-Hill, New York, 1968), Sec. 39.
- <sup>19</sup>H. A. Bethe and E. E. Salpeter, *Quantum Mechanics of One- and Two-Electron Atoms* (Springer, Berlin, 1957), Sec. 6 (parabolic coordinates) and Secs. 3 and 4 (spherical coordinates).
- <sup>20</sup>Hydrogenic ( $F=0$ ) wave functions  $|\epsilon, 0; n_1, m\rangle$  or  $|\epsilon, 0; l, m\rangle$  are usually normalized to unity for  $\epsilon < 0$  and per unit energy for  $\epsilon > 0$ , as in Ref. 19. However, we formally extend the energy normalization to  $\epsilon < 0$  by multiplying  $|\epsilon, 0; n_1, m\rangle$  by  $d\nu/d\epsilon = \nu^3$ ; cf. Eqs. (15) and (17) of this work and Eq. (6.12) of Reference 19; see also Ref. 13, Sec. IID. Moreover, for  $\epsilon = \frac{1}{2}k^2 > 0$  one expects factors like  $(1 \pm e^{-2\pi\beta_l/k})^{-1}$  ( $l=1, 2$ ) to appear in Eqs. (17) and (21), but these would be canceled by like factors in the transformation (18); they have been neglected here for simplicity. They are in fact *replaced* by the factors of  $N_{\epsilon n_1 m}^F$ ; cf. Eqs. (22), (54), and (64). With regard to Stark radiative transitions in H, see also D. R. Herrick, *Phys. Rev. A* 12, 1949 (1975).
- <sup>21</sup>Reference 19, Eqs. (65.4), (63.4), and (71.4).
- <sup>22</sup>R. E. Langer, *Phys. Rev.* 51, 669 (1937).
- <sup>23</sup>D. A. Harmin (unpublished).
- <sup>24</sup>An equipartition rule, due to the equal balancing of the short- and long-range parts of the Coulomb potential, also exists for the stopping power of a free electron gas. See J. Lindhard and A. Winther, *K. Dan. Vidensk. Selsk., Mat.—Fys. Medd.* 34, No. 4 (1964).
- <sup>25</sup>Reference 15, Sec. 52.
- <sup>26</sup>P. F. Byrd and M. D. Friedman, *Handbook of Elliptic Integrals for Engineers and Physicists* (Springer, Berlin, 1954). The complete elliptic integral of the third kind appears here as  $\Pi(\alpha^2, k)$ , where  $\alpha \equiv \alpha^2$ .
- <sup>27</sup>The equation for the *radial* Coulomb wave function  $u(r)$  is
- $$\frac{d^2 u}{d\rho^2} + [1 + (2Z/k)\rho^{-1} - l(l+1)\rho^{-2}]u = 0,$$
- where  $\rho = kr$  and  $\epsilon = \frac{1}{2}k^2$  (for  $\epsilon < 0$  set  $k \rightarrow i/\nu$ ). To obtain Eq. (3b) with  $F=0$  from an equation of this form, one makes the substitutions  $r \rightarrow \eta$ ,  $k \rightarrow \frac{1}{2}k$ ,  $Z \rightarrow \frac{1}{2}\beta_2$ ,  $l \rightarrow \frac{1}{2}(m-1)$ .
- <sup>28</sup>J. O. Hirschfelder and L. A. Curtiss, *J. Chem. Phys.* 55, 1395 (1971); see especially Fig. 4.
- <sup>29</sup>R. E. Langer, *Trans. Am. Math. Soc.* 37, 397 (1935). The results pertinent to this work are given in Ref. 22, Eqs. (31)–(36), for radial parameters  $r, l, Z$ ; the correspondence to  $\eta, m, \beta_2$  follows from Ref. 27.
- <sup>30</sup>In Eqs. (65)–(67), we need only consider those parts of the phase  $\delta_{n_1 m}$  and of the amplitude  $A_{n_1 m}$  which are rapidly varying in energy near the resonance (if  $\epsilon_{n_2} \ll \epsilon_c$ ), i.e.,  $\gamma_{n_1 m}$  and  $R_{n_1 m}$ ; see Ref. 28, Sec. V.
- <sup>31</sup>We have assumed a node of first order. In Ref. 22, Langer addressed the problem of a node of arbitrary order  $\nu$ , whereby the general solutions of Eq. (A1) are Bessel functions of order  $(\nu+2)^{-1}$ .
- <sup>32</sup>Reference 16, Chap. 17, defines  $k^2 \equiv \sin^2 \alpha$ .